

Drag on fixed beds of fibres in slow flow

By I. D. HOWELLS

Department of Mathematics, University of Queensland, 4072 Australia

(Received 20 May 1996 and in revised form 9 September 1997)

As a sequel to earlier work on viscous flow through random beds of fixed spheres, the flow through beds of fixed cylindrical fibres is studied by the same method. Several distributions of orientation are considered. The aim is to find the shielding radius and drag per unit length as a function of volume fraction occupied by the fibres, in the semi-dilute situation. The first approximation is obtained from the drag on a very long cylinder resulting from the uniform flow at infinity of a viscous fluid in the presence of Darcy resistance. Estimates are made of the effects of finite length, and of curvature of the fibres. Finally the effect of a neighbouring cylinder is considered, to obtain the second-stage approximation for straight fibres. Comparison is made with some experimental and numerical results for unidirectional fibres and for plane pads.

1. Introduction

The theoretical treatment of slow flow through fixed beds has been pursued actively since Brinkman (1947) proposed his effective medium and developed the application to the case of spherical objects. Subsequently Spielman & Goren (1968) used the same effective medium to study the drag due to flow through beds of fixed cylinders, with a variety of distributions of orientation. Over the next four years important developments were made in related fields. Batchelor (1971) distinguished dilute and non-dilute (or semi-dilute) suspensions of elongated particles, and introduced a cell model to estimate the stress generated in the latter case by a pure straining motion. Batchelor (1972) showed how to make a re-normalization in order to obtain convergent integrals for the second approximation to the sedimentation velocity of spheres in a dilute dispersion.

Childress (1972) worked out higher approximations to the drag on fixed spheres. For this he made use of two methods, first a process involving interaction diagrams and second, for point forces, an averaged-equation approach with re-normalization. Following on this work, Howells (1974) employed the idea of averaged equations, after extending the flow fields to satisfy the slow flow equations in the interior of the fixed objects. Using Childress's re-normalization technique for the equations, he set up a successive approximation process which is generally applicable to flow in beds of fixed objects, and applied it as far as the third approximation to spheres and to parallel cylinders.

Hinch (1977) discussed very generally the method of averaged equations, and the two kinds of re-normalization. In the application to the fixed bed problem he included dipole contributions on the equations' left-hand side, in such a way as to bypass the need to keep all details of the solution for flow in the effective medium. His solution for the bed of fixed spheres leaves some small unresolved numerical differences with earlier results. Other transport properties of beds and suspensions were studied by Willis & Acton (1976), O'Brien (1979) and Acrivos, Hinch & Jeffrey (1980).

Kaneda (1986) examined the effects of small but finite Reynolds number for flow through a fixed bed of spheres. Having shown that the Oseen drag correction is

dominant when the volume fraction of spheres is of smaller order than the square of the Reynolds number, he calculated the mean drag for the cross-over situation where they are comparable.

In the past ten years there has been a series of papers, including Shaqfeh & Koch (1988), Shaqfeh (1988), Fredrickson & Shaqfeh (1989), Shaqfeh & Fredrickson (1990), Schiek & Shaqfeh (1995), dealing with suspensions and with fixed beds of fibres. These have studied heat flux, hydrodynamic stresses, chemical reactions, particle orientations. The earlier papers used an averaged-equation method, but the 1989 and 1990 papers developed a powerful general formalism using interaction diagrams, to obtain a generalized process of successive approximation that applies to time-dependent as well as steady-state problems. In addition, Frattini *et al.* (1991) and Evans, Shaqfeh & Frattini (1994) have measured some of the predicted effects for comparison with the theory. These papers do not appear to take up directly the question of drag in a fixed bed. It seems that the results they obtained for other mean properties, though obtained in a more general way, are basically analogous to those found for mean drag by the method of averaged equations in Childress (1972) and Howells (1974).

Finally Ghaddar (1995) employed a parallel computational approach to obtain numerical results for the permeability of unidirectional fibrous media. The accuracy achieved by his method does not appear to be high. But within this limitation, and over certain ranges of the volume fraction, he found good agreement with some of the theoretical work, in particular Spielman & Goren (1968) and Howells (1974).

1.1. *Effective medium*

In the effective-medium approach to flow through a fixed bed, the equation for slow viscous flow is modified by an additional term representing a distributed resistance. At its simplest, in the form proposed by Brinkman, this resistance is proportional to the local velocity, according to Darcy's law. The coefficient is obtained theoretically by relating the total drag per unit volume in a uniform mean flow to the drag on an individual element as predicted by the equation for flow in the effective medium.

A critical length is defined by the square root of the ratio of the viscosity to the Darcy coefficient; this separates small-scale viscous motions from large-scale pressure-driven motions that follow Darcy's law. Thus the velocity field due to a point force is approximately a Stokes flow in the near field, and a dipole flow (inverse cube law) in the far field.

It can be seen that the Darcy resistance creates a screening effect. The force is transmitted partly as a pressure field, partly as a field of shear stress, and it is this latter that is screened out over a distance of the order of the critical, or shielding (screening) length.

1.2. *Averaged equations*

In the averaged-equation method, Howells (1974), a series of equations is obtained for successively greater numbers of test objects. For each equation the mean resistance (mean over realizations of the array of objects) is related to an integral of the surface stress on an object in the solution to the succeeding equation in the series. This hierarchy of integro-differential equations is to be truncated, using Darcy's law for the resistance term in the highest-order equation that is to be retained.

1.3. *Interaction diagrams*

The hydrodynamic interactions between objects in a flow can be regarded as a multiple scattering process, and thus represented by a collection of interaction diagrams. Methods of topological reduction have been developed by Childress (1972), Bixon &

Zwanzig (1981), Kirkpatrick (1982), Muthukumar (1982), Fredrickson & Shaqfeh (1989), Shaqfeh & Fredrickson (1990), and others. These methods remove divergences by effectively re-normalizing.

1.4. Orders of magnitude – parameter regimes

In monodisperse beds of fixed spheres, of radius a and number density n , the criterion for a dilute array is that the volume fraction $c = \frac{4}{3}\pi a^3 n$ should be small. With creeping flow, the successive approximation process for the drag on a sphere yields terms of relative order 1, $c^{1/2}$, $c \log c$, c , $c^{3/2} \log c$, ..., where two-body interactions give rise to the $O(c \log c)$ term, and excluded volume effects to an $O(c)$ term.

The extension to elongated objects introduces a much richer set of regimes. The question of curved fibres is left until later; for the moment we consider straight fibres of radius a , half-length l , and number n per unit volume. As a result, a distinction must be made between the dilute regime given by $nl^3 \ll 1$, and the semi-dilute regime with $nl^3 > 1$ and small volume fraction $c (= 2\pi l a^2 n)$. In latter regime the lateral spacing of fibres is small compared to their length.

The present paper is concerned only with the semi-dilute case. But now a further refinement must be introduced, in that hydrodynamic interactions appear as a series of negative powers of $\log 1/c$ whereas the effects of finite thickness, in particular the excluded volume effect, are of order c . In the regime of asymptotically small c the latter effects are exponentially small by comparison with the former.

1.5. Asymptotically small volume fraction

Working in this regime, Howells (1974) gave the drag results from the successive approximation process for infinitely long parallel cylinders. The divisors M_l, M_t (such that the longitudinal and transverse drags per unit length are respectively $2\pi\mu U/M_l, 4\pi\mu U/M_t$) are defined implicitly as functions of the volume fraction:

$$\left. \begin{aligned} 2M_l - \log M_l + 2\gamma - 1.172M_l^{-1} + O(M_l^{-2}) &= \log 2/c, \\ 2M_t - \log M_t + 2\gamma - 0.940M_t^{-1} + O(M_t^{-2}) &= \log 1/c. \end{aligned} \right\} \quad (1.1)$$

Here γ is Euler's constant, and the terms succeeding it on the left-hand side arise from interactions between fibres. A zero-order approximation in each case could be taken as $2M = \log 1/c$, but the attempt to make M the subject of the full equation leads to series in negative powers of $\log 1/c$ together with repeated logarithms. Shaqfeh and his co-authors express some of their results using the first few terms of such a series. It is claimed in the present paper that the implicit formulation of (1.1) is the appropriate one. It retains more nearly the accuracy of which the particular approximation is capable, and it makes clear the order of magnitude of the error made by stopping at a particular point.

In this regime of asymptotically small volume fraction, the interaction diagram method employed by Shaqfeh and his co-authors simplifies, since the fibre thickness is small enough for the fibre probability distributions to be regarded as independent. Their results are derived for such vanishingly small thickness. At the same time the parameter nl^3 is allowed to vary from very large in the asymptotic semi-dilute regime, through large but finite, and through order 1 in the cross-over range, to very small in the asymptotic dilute regime. They consider these regimes in some detail and give results for them all in the problems that are treated.

Section 4 of the present paper considers the effect of small curvature as well as finite length of the fibres. First-approximation calculations are given for the hydrodynamic

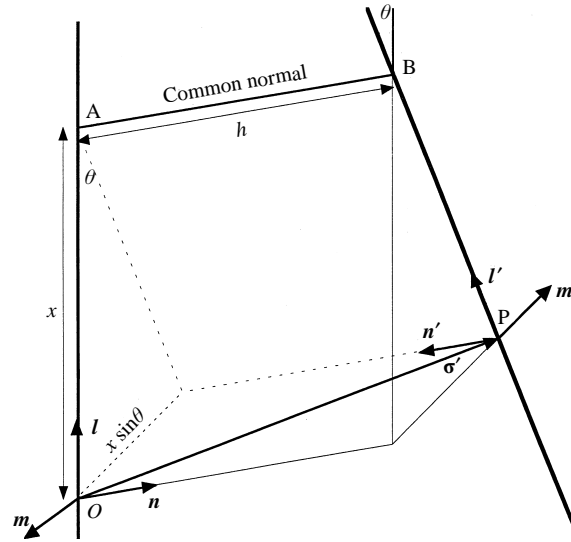


FIGURE 1. Geometry of two straight fibres.

effect of fibre ends on the drag in a fixed bed when nl^3 is large but finite, and then for the correction due to a small curvature of very long fibres.

1.6. Practical values of volume fraction

In the present paper, we relax the asymptotic condition on the volume fraction by letting it take more practical values, say between 0.02 and 0.2. Then c need not be smaller than every negative power of $\log 1/c$ that occurs in the formulae, and a number of effects become significant.

(i) The finite thickness affects the drag formulae at the first approximation. This is seen in the general self-consistency equations for the shielding length, involving modified Bessel functions, as given in Spielman & Goren (1968), Howells (1974), and summarized in §3 of the present paper. The equations corresponding to (1.1) for the first approximation to M_l , M_t (hence omitting the terms after the γ on the left-hand side) are modified by the inclusion of terms of order c .

(ii) When the fibres are of finite length, the Archimedes force makes a contribution to both the transverse and the longitudinal drag coefficients. This force is given by the product of the volume of a fibre and the mean Darcy pressure gradient, and its longitudinal component results from the pressure forces on the fibre ends. The fractional contribution to the drag coefficient is actually equal to c , whatever the fibre length. It is included in the formulae given in §3.

(iii) At the second approximation the excluded-volume effect brings in further terms of order c . In the calculation of this effect it is necessary to take up the question of conditional probability distributions: this is done in §2 of the present paper.

(iv) The hydrodynamic interactions introduce not just negative powers of $\log 1/c$ but also positive powers of c .

1.7. Fibre ends

For clarity we should summarize the conclusions of this paper about the two sources of fibre end effects.

(i) The hydrodynamic effect, resulting from the flow around an end, is significant even for the regime of asymptotically small volume fraction. To the first approximation

for fibre length large but finite, it is proportional to the ratio of shielding length to fibre length (see §4).

(ii) The Archimedes (buoyancy) force, equal to the product of the volume of a fibre and the uniform Darcy pressure gradient, will contribute to the longitudinal as well as the transverse drag, since the fibres have finite length and so in general a pressure difference between the ends. In the earlier treatments it was omitted from the longitudinal drag, on the basis of the model of infinite cylinders. This contribution to the drag is of relative order c , and will be insignificant in the regime of asymptotically small volume fraction.

1.8. Second approximation

The second stage of the approximation process is worked out in §5. It necessarily introduces the interaction between two inclined cylinders, the calculations for which are set out in the Appendices. Results, discussion and comparison with experimental and numerical data are given in §§6–8.

2. Distribution of strands

Given a direction specified by the unit vector \mathbf{l} , and normal to \mathbf{l} a small area dA at \mathbf{r} , the probability that this area is traversed by the axis of a strand having its positive direction within a cone of solid angle $d\Omega(\mathbf{l})$ about \mathbf{l} can be written

$$P(\mathbf{r}, \mathbf{l}) dA d\Omega(\mathbf{l}). \quad (2.1)$$

In an isotropic situation

$$P(\mathbf{r}, \mathbf{l}) = \lambda/(4\pi), \quad (2.2)$$

where λ is the mean length of fibre per unit volume, and hence the volume fraction c is $\pi\lambda a^2$, if the fibres have circular cross-section of radius a .

The conditional probability of another strand at \mathbf{r}' in direction \mathbf{l}' , given one at \mathbf{r} in direction \mathbf{l} , is written in the corresponding way in terms of the density $P(\mathbf{r}', \mathbf{l}' | \mathbf{r}, \mathbf{l})$.

2.1. Probability integrals: approximation of infinite straight strands

Following the iteration scheme set out by Howells (1974), the present paper considers first an isolated test strand in Brinkman's medium, and then the effect of a second test strand. So that the second stage calculations may be manageable, we make the approximation of infinite straight test strands. The effect is then averaged over all positions of the second strand.

With no loss of generality, choose the origin of position vectors so that $\mathbf{r} = 0$, and specify the position vector \mathbf{r}' of the second strand uniquely by the requirement that it be perpendicular to \mathbf{l} : then it is written $\boldsymbol{\sigma}' = \mathbf{m}'y' + \mathbf{n}'z'$. The differential element of probability becomes

$$P(\boldsymbol{\sigma}', \mathbf{l}' | 0, \mathbf{l}) dA(\boldsymbol{\sigma}') d\Omega(\mathbf{l}').$$

The element of area $dA(\boldsymbol{\sigma}')$ (invariant under reversal of the sign convention for $\boldsymbol{\sigma}'$) is written in general as either $dy' dz'$ or $\boldsymbol{\sigma}' d\boldsymbol{\sigma}' d\phi'$. But in the calculation of the mean value of the interaction between the two rods, it can also be expressed as follows in terms of the geometry of the two rods. Orthogonal triads of unit vectors $\mathbf{l}, \mathbf{m}, \mathbf{n}$ and $\mathbf{l}', \mathbf{m}', \mathbf{n}'$ are as shown in figure 1, where $\mathbf{n} = -\mathbf{n}'$ is normal to both axes. The position on the \mathbf{l} -axis of the foot of the common normal is denoted by x , and the length of the common normal by h . Spherical polars θ, ϕ are used for \mathbf{l}' , with \mathbf{l} as the pole. Then

$$\left. \begin{aligned} \boldsymbol{\sigma}' &= \mathbf{m}'x \sin \theta + \mathbf{n}h, \\ dA(\boldsymbol{\sigma}') &= \sin \theta dh dx, \\ d\Omega(\mathbf{l}') &= \sin \theta d\theta d\phi. \end{aligned} \right\} \quad (2.3)$$

If h is restricted to be positive, the range of θ is from $-\pi$ to π . Thus if a quantity f depends on the position of the second strand, its expected value is

$$\langle f \rangle = \int_{-\pi}^{\pi} \sin^2 \theta \, d\theta \int_0^{2\pi} d\phi \int_0^{\infty} dh \int_{-\infty}^{\infty} f P(\boldsymbol{\sigma}', l' | 0, l) \, dx. \quad (2.4)$$

2.2. Conditional probability density

The simplest consistent form of the conditional probability density is found in a constructive way as follows (see Clague & Phillips 1996, §II C). Let a random isotropic distribution of infinite cylinders be given, with overlaps being permitted. Then at each overlap, let the axes of the two strands involved be deformed in such a way that the overlap is removed, leaving just one point of contact between the strands. An appropriate spline shape for the deformation can be assigned: for a given volume fraction it should take up a prescribed length, and have a correspondingly determined maximum curvature for the situation of greatest possible overlap. The deformations will of course introduce new overlaps: these are to be removed in the same way, and so on. It can be seen that for a sufficiently large permitted maximum curvature, depending on the volume fraction of thread, the process can be a convergent one, leading to a limiting distribution without overlaps.

It is now necessary to determine the resulting form for $P(\boldsymbol{\sigma}', l' | 0, l)$, so as to estimate the interaction between strands. In the approximation needed for this estimate, the above procedure is modified for the two infinite test cylinders that are notionally inserted into a Brinkman's medium. If they intersect, it will be adequate for the interaction estimate to suppose that they are not deformed but simply translated by equal amounts in opposite directions until they just touch. Then, assuming isotropy, the conditional probability density depends on the length of the common normal h as follows:

$$P(\boldsymbol{\sigma}', l' | 0, l) = \lambda / (4\pi) \{u(h-2a) + 2a\delta(h-2a)\},$$

where $u(h-2a)$ is the unit step function, and the delta-function corresponds to the accumulated probability of initially intersecting strands that have been displaced.

When this is inserted into (2.4), the expected value is

$$\langle f \rangle = \frac{\lambda}{4\pi} \int_{-\pi}^{\pi} \sin^2 \theta \, d\theta \int_0^{\infty} \{u(h-2a) + 2a\delta(h-2a)\} \, dh \int_0^{2\pi} d\phi \int_{-\infty}^{\infty} f \, dx. \quad (2.5)$$

In the actual calculation f denotes a contribution to the force per unit length on the first cylinder. The value of f at a point depends on the distance x of that point from the foot of the common normal; hence the x -integral in (2.5) is equal to the corresponding contribution to the total force on the first cylinder.

3. First approximation: drag on one very long test cylinder

At the first approximation, the drag per unit length of fibre is calculated for the limiting case of a very long circular cylinder. Being finite, as explained in §1, the cylinder experiences the longitudinal as well as the transverse component of buoyancy force, given by the product of its volume and the mean pressure gradient. This requires a modification to the longitudinal drag coefficient given in earlier work, which was based on the model of an infinite cylinder.

In the flow equation for Brinkman's effective medium (omitting average signs) we

denote the Darcy coefficient k by $\mu\alpha^2$ for the sake of simplicity in the expressions for the Green's function. Then α^{-1} is the shielding radius:

$$\left. \begin{aligned} -\nabla p + \mu\nabla^2 \mathbf{u} &= \mu\alpha^2 \mathbf{u}, \\ \nabla \cdot \mathbf{u} &= 0. \end{aligned} \right\} \quad (3.1)$$

From Howells (1974, equation (4.7)), solutions are conveniently expressed in terms of the elementary solution, the 'shielded Stokeslet' of strength \mathcal{S} :

$$\mathbf{u}(\mathbf{r}) = \mathcal{S} \cdot \mathcal{J}(\mathbf{r}),$$

$$\text{where} \quad \mathcal{J}(\mathbf{r}) = (\nabla\nabla - I\nabla^2) 2\alpha^{-2} r^{-1} (1 - e^{-\alpha r}) \quad (3.2)$$

is the (three-dimensional) Green's function.

For the purpose of the Section on curved threads, it is convenient to make use as well of the elementary rotational solution ('rotlet') of strength \mathcal{M} :

$$\mathbf{u}(\mathbf{r}) = \nabla \times \{\mathcal{M} \cdot \mathcal{J}(\mathbf{r})\} = -\mathcal{M} \times \nabla (2r^{-1} e^{-\alpha r}). \quad (3.3)$$

The flow due to a force field $\mathcal{Q}(\mathbf{r})$ acting on the fluid is given by the volume integral:

$$\mathbf{u}(\mathbf{r}) = (8\pi\mu)^{-1} \int \mathcal{Q}(\mathbf{r}') \cdot \mathcal{J}(\mathbf{r} - \mathbf{r}') d\mathbf{r}'. \quad (3.4)$$

Then the Green's function for a cylindrical flow (independent of the axial coordinate x), is obtained by integrating (3.2) along the axis, with the result

$$\mathcal{J}_t(\mathbf{r}) = (\nabla\nabla - I\nabla^2) 2\alpha^{-2} \{-\log \alpha\sigma - K_0(\alpha\sigma)\}. \quad (3.5)$$

Howells (1974) also sets out the Faxén's formulae for longitudinal and transverse drag per unit length on an infinite cylinder in an externally produced velocity field $\mathbf{u}_e(\boldsymbol{\sigma})$ (independent of x). The formulae can be combined into one expression for a cylinder having radius a , and its axis in direction \mathbf{l} :

$$\mathbf{f}(\mathbf{l}) = 4\pi\mu \{ \mathbf{C}_0(\mathbf{l}) + \mathbf{C}_2(\mathbf{l}) a^2 \nabla^2 \} \cdot \mathbf{u}_e(0), \quad (3.6)$$

in terms of the tensor coefficients

$$\mathbf{C}_0(\mathbf{l}) = C_L \mathbf{l}\mathbf{l} + C_T (\mathbf{I} - \mathbf{l}\mathbf{l}), \quad \alpha^2 a^2 \mathbf{C}_2(\mathbf{l}) = C_S (\mathbf{I} - \frac{1}{2} \mathbf{l}\mathbf{l}) - \mathbf{C}_0(\mathbf{l}),$$

where

$$C_S = 1/K_0(\alpha a), \quad C_L = \frac{1}{2} \alpha a K_1(\alpha a)/K_0(\alpha a),$$

$$C_T = \frac{1}{2} \alpha^2 a^2 K_2(\alpha a)/K_0(\alpha a) = \alpha a K_1(\alpha a)/K_0(\alpha a) + \frac{1}{2} \alpha^2 a^2.$$

In the present paper the formula for longitudinal drag needs modification for the case of uniform flow at infinity, so as to include the force due to the pressure difference between the ends of a long but finite rod, as already explained. When this is done, the drag per unit length on a long cylinder with uniform velocity \mathbf{U} at infinity becomes

$$\begin{aligned} \mathbf{f}^*(\mathbf{l}) &= 4\pi\mu \{ \mathbf{C}_0(\mathbf{l}) + \frac{1}{4} \alpha^2 a^2 \mathbf{l}\mathbf{l} \} \cdot \mathbf{U} \\ &= 4\pi\mu \mathbf{C}_0^*(\mathbf{l}) \cdot \mathbf{U} \\ &= 4\pi\mu C_T (\mathbf{I} - \frac{1}{2} \mathbf{l}\mathbf{l}) \cdot \mathbf{U}. \end{aligned} \quad (3.7)$$

Let λ be the mean length of filament, measured along the axis, per unit volume, and so $c = \pi\lambda a^2$ is the volume fraction of filaments. Since the medium is supposed to be isotropic the angular distribution of \mathbf{l} must also be isotropic, and the mean value of $\mathbf{l}\mathbf{l}$ over all directions is $\frac{1}{3} \mathbf{I}$. Then the self-consistency equation for α is

$$\mu\alpha^2 \mathbf{U} = \frac{\lambda}{4\pi} \int \mathbf{f}^*(\mathbf{l}) d\Omega(\mathbf{l}) = \mu\lambda C_T \int (\mathbf{I} - \frac{1}{2} \mathbf{l}\mathbf{l}) \cdot \mathbf{U} d\Omega(\mathbf{l}) = \frac{10}{3} \pi\mu\lambda C_T \mathbf{U},$$

which reduces to

$$K_0(\alpha a)/K_2(\alpha a) = \frac{5}{3}c. \quad (3.8)$$

Compare the equations for random arrays of parallel rods:

$$\left. \begin{array}{l} \text{Longitudinal flow}^\dagger \quad \alpha a K_0(\alpha a)/K_1(\alpha a) = 2c, \\ \text{Longitudinal flow}^* \quad K_0(\alpha a)/K_2(\alpha a) = c, \\ \text{Transverse flow} \quad K_0(\alpha a)/K_2(\alpha a) = 2c, \end{array} \right\} \quad (3.9)$$

where \dagger denotes the absence of pressure forces on the ends, and $*$ their inclusion.

Note that it is only at the first stage, for one test cylinder, that the modification for end pressure forces must be made. After that, any pressure difference between the ends, associated with higher-order disturbance flow fields, tends to zero as the fibre length tends to infinity.

These differences in the self-consistency equation for longitudinal flow, between infinite cylinders and very long finite cylinders, seem paradoxical. Of course the ambiguity in the drag formula can be explained physically, but it does not seem that the shielding radius should be affected by the presence or absence of ends, when the threads are very long. Presumably the paradox is inherent in the successive approximation process, which is capable of giving a unique result from different starting points.

3.1. Fibre pads

The above results for longitudinal flow through parallel arrays (without pressure forces on the ends), and flow through arrays randomly orientated in three dimensions, agree with Spielman & Goren (1968). But these authors also consider a pad of fibres randomly orientated in the plane of the pad. The Darcy law is now anisotropic: flow normal to the pad is normal to all the fibre axes, whereas flow in the plane of the pad meets fibres in all oblique directions. The exact first-order theory is complicated mathematically. The authors neglect the anisotropy in their solution for flow round a fibre, and their equation for the Darcy resistance coefficient for flow normal to the pad is the same as for the case of parallel fibres. On the other hand, the equation for flow in the plane of the pad involves averaging over all directions of the fibres, and takes the form

$$\alpha^2 a^2 = 2c(C_T + C_L) = c\{3\alpha a K_1(\alpha a)/K_0(\alpha a) + \alpha^2 a^2\},$$

i.e.

$$(2+c)K_0(\alpha a)/K_2(\alpha a) = 3c.$$

It can be seen that on the initial approximation, and for very small volume fraction, the ratio of resistance normal to and parallel to the plane of the pad is 4:3.

Although it is not convenient to carry out an exact solution for flow past a cylinder in an anisotropic Brinkman medium, it is fairly simple to find a first correction to the initial approximation. Given the (two-dimensional) flow field for an isotropic medium, the unbalanced resistance field due to the anisotropy can be written as the right-hand side of Brinkman's equation. Then the first correction field and drag on the cylinder are determined using the isotropic Green's function. If $\alpha^2 a^2$ is taken as the average of $\alpha_1^2 a^2$ and $\alpha_2^2 a^2$, corresponding to drag normal to and parallel to the plane of the pad, and C_L, C_T are as defined in terms of αa after equation (3.6), the self-consistency equations are given to this approximation by

$$\alpha^2 a^2(1 + \frac{1}{4}c) = \frac{7}{2}cC_T, \quad \text{i.e.} \quad (1 + \frac{1}{4}c)K_0(\alpha a)/K_2(\alpha a) = \frac{7}{4}c,$$

and

$$\alpha_1^2 a^2/\alpha^2 a^2 = 1 + (1+2c)/\{7(1+c) - (4-6c)C_L\}.$$

4. Effects of finite length and of curvature

4.1. Finite length, in the semi-dilute regime

Consider first the hydrodynamic effect of the ends of straight fibres. If there are n fibres per unit volume, the mean length is $l_m = \lambda/n$. It can be seen that the maximum possible value of l_m is double the expected distance a rod of radius a can be extended from a given point, before meeting another rod. For random distributions it is found that

$$(l_m)_{max} = 2/(\pi a \lambda) = 2a/c. \quad (4.1)$$

Consideration is restricted to the case where l_m is large compared to the shielding radius. In combination with (4.1), this restriction can be stated as

$$\alpha a \gg a/l_m > \frac{1}{2}c. \quad (4.2)$$

In this situation each fibre end can be regarded as adding approximately the same amount to the total effective length per unit volume, to be calculated as for a semi-infinite rod. Since the disturbance flow due to an infinite rod corresponds to a line distribution of singularities (shielded Stokeslets) along the axis, the flow past a semi-infinite rod can be found (for small αa) by successive approximations, starting with the flow that results by the omission of the singularities along one half of the axis ($x < 0$). The first-order remainder flow at $x > 0$ is

$$\begin{aligned} U \cdot \mathbf{I} C_L \left[\alpha^{-2} x^{-2} \{1 - (1 + \alpha x) e^{-\alpha x}\} + \int_x^\infty e^{-\alpha x'} x'^{-1} dx' \right] \\ + U \cdot (\mathbf{I} - \mathbf{I}) \frac{1}{2} C_T \left[-\alpha^{-2} x^{-2} \{1 - (1 + \alpha x) e^{-\alpha x}\} + \int_x^\infty e^{-\alpha x'} x'^{-1} dx' \right]. \end{aligned}$$

The first correction to the drag per unit length at x is obtained by treating the remainder flow at any x as a uniform flow, and applying the factor $\mathbf{C}_0(\mathbf{I})$. Then

$$\begin{aligned} f_1(x) = 4\pi\mu U \cdot \mathbf{I} C_L^2 \left[\alpha^{-2} x^{-2} \{1 - (1 + \alpha x) e^{-\alpha x}\} + \int_x^\infty e^{-\alpha x'} x'^{-1} dx' \right] \\ + 2\pi\mu U \cdot (\mathbf{I} - \mathbf{I}) C_T^2 \left[-\alpha^{-2} x^{-2} \{1 - (1 + \alpha x) e^{-\alpha x}\} + \int_x^\infty e^{-\alpha x'} x'^{-1} dx' \right]. \end{aligned}$$

When these are integrated, the total additional force near the end of the rod is obtained:

$$\mathbf{F}_e = 8\pi\mu\alpha^{-1} U \cdot [\{C_L^2 + O(\alpha a)\} \mathbf{I} + O(\alpha a) (\mathbf{I} - \mathbf{I})]. \quad (4.3)$$

The added effective length per fibre end is thus to leading approximation:

$$\begin{aligned} 4\alpha^{-1} C_L^2 / C_T & \text{ for longitudinal flow,} \\ 0 & \text{ for transverse flow.} \end{aligned}$$

The self-consistency equation is, to the same approximation,

$$\begin{aligned} \alpha^2 a^2 &= \frac{10}{3} c C_T + \frac{16}{3} \pi a^2 n \alpha^{-1} C_L^2 \\ &= \frac{10}{3} c C_T \{1 + \frac{8}{5} (\alpha l_m)^{-1} C_L^2 / C_T\}. \end{aligned} \quad (4.4)$$

4.2. Curved thread: complete circle

Given a length of fibre in the form of a ring of radius $R \gg \alpha^{-1}$, in a flow U at infinity, the effect of curvature on the drag at any point is to be calculated to the first approximation. Take the origin O on the fibre axis, and measure angle θ around the

ring from O . The orthonormal reference triad at O is \mathbf{i} (tangential), \mathbf{j} (radially inwards), \mathbf{k} , and the corresponding triad at angle θ is $\mathbf{l}, \mathbf{m}, \mathbf{k}$. The leading approximation to the drag at θ is $\mathbf{f} = -4\pi\mu C_T(\mathbf{I} - \frac{1}{2}\mathbf{ll}) \cdot \mathbf{U}$.

Represent the disturbance flow due to the circle in terms of a combined distribution of shielded Stokeslets and 'rotlets' (equation (3.3)) around the circular axis of the fibre. Let $\boldsymbol{\sigma}$ be the position vector of a point P in the plane $\theta = 0$, and let \mathbf{r}' be the position vector of a point Q at angle θ on the fibre axis. The disturbance velocity field is

$$\mathbf{u}(\mathbf{r}) = (\nabla\nabla - I\nabla^2) \cdot \boldsymbol{\Phi}(\mathbf{r}) + \nabla \times \mathbf{X}(\mathbf{r}), \quad (4.5)$$

where

$$\alpha^2 \boldsymbol{\Phi}(\mathbf{r}) = - \int_{-\pi}^{\pi} \mathbf{U} \cdot \{\mathbf{A} - \mathbf{B} \exp(-\alpha|\mathbf{r} - \mathbf{r}'|)\} \frac{R d\theta}{|\mathbf{r} - \mathbf{r}'|},$$

$$\mathbf{X}(\mathbf{r}) = \int_{-\pi}^{\pi} \mathbf{U} \cdot \mathbf{B}_r \exp(-\alpha|\mathbf{r} - \mathbf{r}'|) \frac{R d\theta}{|\mathbf{r} - \mathbf{r}'|},$$

with

$$\mathbf{A}(\theta) = (A_1 \mathbf{ll} + A_2 \mathbf{mm} + A_3 \mathbf{kk}), \quad \mathbf{B}(\theta) = (B_1 \mathbf{ll} + B_2 \mathbf{mm} + B_3 \mathbf{kk}),$$

$$\mathbf{B}_r(\theta) = (B_{r1} \mathbf{lk} + B_{r3} \mathbf{kl}).$$

Here the second integral arises from the 'rotlet' distribution: a main velocity in the plane of the ring produces rotational effects in that plane (except at points where the velocity is normal to the thread), and perpendicular to the plane of the ring it produces rotational effects about the circular axis of the fibre.

These tensors are to be expressed in terms of $\mathbf{i}, \mathbf{j}, \mathbf{k}$ and the angle θ . Since terms that are odd functions of θ do not contribute to the integral, the tensor \mathbf{A} is replaced by $(A_1 \mathbf{ii} + A_2 \mathbf{jj} + A_3 \mathbf{kk}) + (\mathbf{ii} - \mathbf{jj})(A_2 - A_1) \sin^2 \theta$, and similarly for \mathbf{B} .

Expressions for $\boldsymbol{\Phi}(\mathbf{r}), \mathbf{X}(\mathbf{r})$ are first found on the axial plane $\theta = 0$, as functions of $\boldsymbol{\sigma} = y\mathbf{j} + z\mathbf{k}$, and then extended to general points using the axisymmetry of the ring. They are calculated as expansions in powers of $y/R, z/R$, using the relation

$$|\boldsymbol{\sigma} - \mathbf{r}'| = (r'^2 + \sigma^2)^{1/2} \{1 - (y/R) r'^2 / (r'^2 + \sigma^2)\}^{1/2}.$$

The relevant differential operators in (4.5) are applied to $\boldsymbol{\Phi}(\mathbf{r}), \mathbf{X}(\mathbf{r})$ to obtain the resulting disturbance velocity field \mathbf{U}_a , and hence the remainder velocity field $\mathbf{U} + \mathbf{U}_a$ at the surface of the fibre.

When the first approximations are used for \mathbf{A}, \mathbf{B} , namely $C_T(\mathbf{I} - \frac{1}{2}\mathbf{ll}), C_S(\mathbf{I} - \frac{1}{2}\mathbf{ll})$ respectively, and the term in R^{-1} is eliminated by the 'rotlet' distribution

$$\mathbf{B}_r = (a/R) \{\alpha a K_1(\alpha a)\}^{-1} (\frac{1}{4}\mathbf{lk} + \frac{3}{4}\mathbf{kl}),$$

the remainder flow on the fibre surface is obtained to leading order of approximation, at a general point on the circle:

$$\begin{aligned} \mathbf{U} + \mathbf{U}_a = & \frac{1}{8}(\alpha R)^{-2} \mathbf{U} \cdot [(-2C_L + 4\alpha^2 a^2 - 9\alpha^2 y^2 - 3\alpha^2 a^2 / C_L) \mathbf{ll} \\ & + \{-(6 \log 8R/a - 7) C_T + 6 - 3\alpha^2 a^2 + 6\alpha^2 y^2 + 6\alpha^2 a^2 / C_L\} \mathbf{mm} \\ & + \{(2 \log 8R/a - 5) C_T - 2 + \alpha^2 a^2 / C_L\} \mathbf{kk}]. \end{aligned}$$

This is to be eliminated by combinations of the standard solutions for a cylinder. Finally a stress calculation leads to the expression for the total drag, to the same approximation:

$$\begin{aligned} \mathbf{f} = & 4\pi\mu C_T(\mathbf{I} - \frac{1}{2}\mathbf{ll}) \cdot \mathbf{U} + \frac{1}{4}\pi\mu(\alpha R)^{-2} \mathbf{U} \cdot [(-C_T^2 + 6\alpha^2 a^2 + \frac{1}{4}\alpha^4 a^4 + \frac{3}{2}\alpha^4 a^4 / C_L) \mathbf{ll} \\ & + 4C_T(C_T \log 8R/a - 1)(-3\mathbf{mm} + \mathbf{kk}) + (11C_T^2 - \alpha^2 a^2 C_T + \frac{1}{8}\alpha^4 a^4)(\mathbf{mm} - \mathbf{kk}) \\ & + (C_T^2 + 4\alpha^2 a^2 + \frac{1}{2}\alpha^4 a^4 + \alpha^4 a^4 / C_L)(3\mathbf{mm} + \mathbf{k})]. \end{aligned} \quad (4.6)$$

4.3. Circular arc between straight sections

Consider next a circular arc of the same radius, together with the semi-infinite straight pieces tangent to the arc at its ends, provided the arclength is large compared with the shielding radius. The difference between the additional drag in this case and the case of the circle is more readily found, since the effect of the portions of fibre beyond the ends of the arc can be treated as a pressure-driven flow, and terms in $\exp(-\alpha r)$ neglected. It is found that the expression

$$\frac{1}{4}\pi\mu(\alpha R)^{-2}U \cdot [28C_L C_T \mathbf{ll} - 27C_T^2 \mathbf{mm} + 3C_T^2 \mathbf{kk} - 4C_T^2(\log 4R/l_{ch})(-3\mathbf{mm} + \mathbf{kk})],$$

where l_{ch} is the chord length of half of the circular arc, is to be added to (4.6), with the result

$$\begin{aligned} \mathbf{f} = & 4\pi\mu C_T (\mathbf{I} - \frac{1}{2}\mathbf{ll}) \cdot U \\ & + \frac{1}{4}\pi\mu(\alpha R)^{-2}U \cdot [(13C_T^2 - 7\alpha^2 a^2 C_T + 6\alpha^2 a^2 + \frac{1}{4}\alpha^4 a^4 + \frac{3}{2}\alpha^4 a^4 / C_L) \mathbf{ll} \\ & + 4C_T(C_T \log 2l_{ch}/a - 1)(-3\mathbf{mm} + \mathbf{kk}) + (2C_T^2 - \alpha^2 a^2 C_T + \frac{1}{8}\alpha^4 a^4)(\mathbf{mm} - \mathbf{kk}) \\ & + (-5C_T^2 + 4\alpha^2 a^2 + \frac{1}{2}\alpha^4 a^4 + \alpha^4 a^4 / C_L)(3\mathbf{mm} + \mathbf{kk})]. \end{aligned}$$

The mean drag as the plane of the circle is rotated about \mathbf{l} , when R^{-2} denotes the mean-square curvature, is given to the same approximation by

$$4\pi\mu C_T U \cdot \{[\frac{1}{2} + (\alpha R)^{-2} f_{c1}(\alpha a)] \mathbf{ll} + \{1 + (\alpha R)^{-2} f_{c2}(\alpha a, l_{ch}/a)\} (\mathbf{I} - \mathbf{ll})\}, \quad (4.7)$$

where

$$\begin{aligned} f_{c1}(\alpha a) &= \frac{1}{16} \{13C_T - 7\alpha^2 a^2 + (\alpha^2 a^2 / C_T) (6 + \frac{1}{4}\alpha^2 a^2 + \frac{3}{2}\alpha^2 a^2 / C_L)\}, \\ f_{c2}(\alpha a, l_{ch}/a) &= \frac{1}{16} \{-4C_T \log 2l_{ch}/a - 10C_T + 4 + (\alpha^2 a^2 / C_T) (8 + \alpha^2 a^2 + 2\alpha^2 a^2 / C_L)\}. \end{aligned}$$

4.4. Random fibre configuration

In the case where the tangent vector \mathbf{l} is a stationary random function of the arclength s , an additional effect is an increase in the conditional probability of fibres within a radius L of a given point P through which the thread passes (omitting the region of high probability close to the straight line through P in direction $\mathbf{l}(0)$). The correlation coefficient can be defined as $\langle \mathbf{l}(0) \cdot \mathbf{l}(s) \rangle$, and L will be the integral length scale. The mean length of fibre per unit volume at distance r from P can be expressed as $\lambda + \Delta\lambda$, where $\Delta\lambda = L^{-2} A(r)$. At large distances $A(r) \approx 3L/(2\pi r)$; provided L is large compared to the shielding radius this function can be treated as having constant value $A(0) \approx 3/(2\pi)$ in the neighbourhood of P .

Use of the self-consistency equation (3.9) permits determination of the local change in shielding radius, i.e. in the Darcy coefficient $k = \mu\alpha^2$, as a result of this small local increase in thread length per unit volume. The result is found to be

$$\Delta(\alpha^2) \approx L^{-2} J C_T^2 / (C_T - 2C_L^2), \quad (4.8)$$

where

$$J = \frac{10}{3}\pi A(0) \approx 5.$$

This local increase in the Darcy coefficient interacts with the main flow and also with the disturbance flow due to that portion of the thread near P that can be regarded as straight. The result is a remainder flow at P , giving the leading approximation to the additional drag due to the conditional probability effect:

$$\delta\mathbf{f} = 4\pi\mu(\alpha L)^{-2} C_T U \cdot \{f_{r1}(\alpha a) \mathbf{ll} + f_{r2}(a) (\mathbf{I} - \mathbf{ll})\}, \quad (4.9)$$

where (see (4.8))

$$\begin{aligned} f_{r1}(\alpha a) &= \{J C_T / (C_T - 2C_L^2)\} [-\frac{1}{3}C_T + C_L^2 - \frac{1}{4}\alpha^2 a^2 + \frac{1}{12}(C_S - C_T) \{3C_T - 7 - O(\alpha^2 a^2)\}], \\ f_{r2}(a) &= \{J C_T / (C_T - 2C_L^2)\} [-\frac{2}{3}C_T + 2C_L^2 - \frac{3}{10}\alpha^2 a^2 + \frac{1}{6}(C_S - C_T) \{3C_T - 7 - O(\alpha^2 a^2)\}], \end{aligned}$$

and note that $(C_S - C_T) = \frac{1}{4}\alpha^2 a^2 / K_0(\alpha a) + O(\alpha^4 a^4)$.

αa	C_L	C_T	c_1	$4C_L^2/C_T$	$f_{c_1}(\alpha a)$	$f_{c_2}(\alpha a, 4)$	$f_{c_3}(\alpha a, 8)$	$f_{c_3}(\alpha a, 16)$	$f_{r_1}(\alpha a)$	$f_{r_2}(\alpha a)$
0.01	0.1059	0.2118	0.0001416	0.2117	0.1722	0.00775	-0.02895	-0.06565	-0.3323	-0.6644
0.02	0.1240	0.2482	0.000483	0.2478	0.2021	-0.03336	-0.07637	-0.1194	-0.3851	-0.7696
0.05	0.1598	0.3209	0.002337	0.3184	0.2626	-0.1135	-0.1691	-0.2247	-0.4885	-0.9735
0.1	0.2030	0.4110	0.007299	0.4011	0.3388	-0.2082	-0.2794	-0.3506	-0.6179	-1.2201
0.2	0.2725	0.5650	0.02124	0.5257	0.4691	-0.3600	-0.4579	-0.5558	-0.8600	-1.6467
0.4	0.3920	0.8640	0.05556	0.7114	0.7090	-0.6352	-0.7849	-0.9346	-1.4834	-2.5748
0.6	0.5027	1.1854	0.09111	0.8527	0.9416	-0.9212	-1.1266	-1.3320	-2.5001	-3.8198
0.8	0.6097	1.5395	0.12472	0.9660	1.1718	-1.2334	-1.5002	-1.7670	-4.1987	-5.5844

TABLE 1. Correction functions $4C_L^2/C_T, f_{c_1}(\alpha a), f_{c_2}(\alpha a, l_{ch}/a), f_{r_1}(\alpha a), f_{r_2}(\alpha a)$, in the generalized drag formula (4.10), for threads of mean length l_m , for threads with mean-square curvature R^{-2} and half-chord length l_{ch} , and for randomly configured threads with integral length scale L .

αa	c_1	$\frac{8}{3}C_L^2/C_T$	$\frac{2}{3}f_{c_1}(\alpha a) + \frac{1}{3}f_{c_2}(\alpha a, 4)$	$\frac{2}{3}f_{c_1}(\alpha a) + \frac{1}{3}f_{c_2}(\alpha a, 8)$	$\frac{2}{3}f_{c_1}(\alpha a) + \frac{1}{3}f_{c_2}(\alpha, 16)$	$\frac{2}{3}f_{r_1}(\alpha a) + \frac{1}{3}f_{r_2}(\alpha a)$
0.01	0.0001416	0.0847	0.0751	0.0457	0.0164	-0.6644
0.02	0.000483	0.0991	0.0542	0.0197	-0.0147	-0.7697
0.05	0.002337	0.1274	0.0142	-0.0302	-0.0747	-0.9742
0.1	0.007299	0.1604	-0.0310	-0.0880	-0.1450	-1.2232
0.2	0.02124	0.2103	-0.1003	-0.1786	-0.2570	-1.6613
0.4	0.05556	0.2845	-0.2246	-0.3444	-0.4641	-2.6532
0.6	0.09111	0.3411	-0.3603	-0.5247	-0.6890	-4.0559
0.8	0.12472	0.3864	-0.5180	-0.7315	-0.9449	-6.147

TABLE 2. Correction functions $\frac{8}{3}C_L^2/C_T, \frac{2}{3}f_{c_1}(\alpha a) + \frac{1}{3}f_{c_2}(\alpha a, l_{ch}/a), \frac{2}{3}f_{r_1}(\alpha a) + \frac{1}{3}f_{r_2}(\alpha a)$, in the self-consistency equation (4.11) determining the parameter αa as a function of the volume fraction c .

4.5. *Summary of results for a single fibre*

The results of §§3 and 4, equations (3.8), (4.3), (4.7), (4.9), can now be brought together in the expression for mean drag per unit length

$$\begin{aligned} \mathbf{f} = 4\pi\mu C_T \mathbf{U} \cdot [\mathbf{I} - \frac{1}{2}\mathbf{U}\mathbf{U} + (\alpha l_m)^{-1} 4C_L^2/C_T \mathbf{U}\mathbf{U} + (\alpha R)^{-2} \{f_{c1}(\alpha a)\mathbf{U}\mathbf{U} + f_{c2}(\alpha a, l_{ch}/a)(\mathbf{I} - \mathbf{U}\mathbf{U})\} \\ + (\alpha L)^{-2} \{f_{r1}(\alpha a)\mathbf{U}\mathbf{U} + f_{r2}(\alpha a)(\mathbf{I} - \mathbf{U}\mathbf{U})\}], \end{aligned} \quad (4.10)$$

and the self-consistency equation, following the pattern of (3.9)

$$\begin{aligned} K_0(\alpha a)/K_2(\alpha a) = \frac{5}{3}c[1 + (\alpha l_m)^{-1} \frac{8}{5}C_L^2/C_T + (\alpha R)^{-2} \{\frac{2}{5}f_{c1}(\alpha a) + \frac{4}{5}f_{c2}(\alpha a, l_{ch}/a)\} \\ + (\alpha L)^{-2} \{\frac{2}{5}f_{r1}(\alpha a) + \frac{4}{5}f_{r2}(\alpha a)\}]. \end{aligned} \quad (4.11)$$

Here the four terms in the square bracket correspond to: very long straight fibres, the effect of finite mean length l_m , the effect of mean-square curvature R^{-2} with correlation length l_{ch} for the curvature, and the effect of local increase in fibre density with a random configuration of fibre on length scale L . Numerical values of the functions involved are shown in tables 1 and 2.

5. Second-stage drag calculation (two test cylinders)

5.1. *Successive approximation scheme*

The general scheme for spheres is set out in Howells (1974, §5). In the case of m ‘test spheres’ in prescribed positions, the flow field is expressed as the sum of the main flow and a collection of ‘difference flows’, one for each subset of the test spheres. This scheme applies equally to obstacles of any shape provided that, in specifying the flow variables, additional arguments are included to describe the orientation (and size and shape if necessary) of the obstacles.

In this paper, if the calculation of interactions between nearby threads is to be practicable, even as far as $m = 2$, it is necessary to use the approximation of test obstacles in the form of infinite straight rods. Then the only additional argument required for each rod is the unit vector giving its direction.

5.2. *One test rod*

The test rod is in the direction of the unit vector \mathbf{l} , and the cylinder axis passes through the origin. The coordinates are those given in §3, and as follows:

position vectors

$$\begin{aligned} \mathbf{r} = x\mathbf{l} + \boldsymbol{\sigma} \quad (\boldsymbol{\sigma} \cdot \mathbf{l} = 0) \quad \text{for a general point,} \\ \mathbf{r} = x\mathbf{l} + \mathbf{a} \quad (|\mathbf{a}| = a, \mathbf{a} \cdot \mathbf{l} = 0) \quad \text{for a point on surface of rod;} \end{aligned}$$

element of length around circumference of a normal section
 $dL(\mathbf{a})$.

For the disturbance flow field set up by the cylinder, the important mean quantities are

mean disturbance velocity field $U_i(\mathbf{r}; \mathbf{l})$,

mean disturbance resistance force acting on fluid $R_1(\mathbf{r}; \mathbf{l})$,

mean discontinuity in stress across surface of rod at $x\mathbf{l} + \mathbf{a}$ $T_1(x, \mathbf{a}; \mathbf{l})$,

mean drag force per unit length of rod $\mathbf{f}_1^*(\mathbf{l}) = \oint T_1(x, \mathbf{a}; \mathbf{l}) dL(\mathbf{a}) + \pi\mu\alpha^2 a^2 \mathbf{l} \cdot \mathbf{U}$,

where the second term is the longitudinal buoyancy pressure force on a very long finite rod, as discussed in §1. By homogeneity, all of these quantities except $T_1(x, \mathbf{a}; \mathbf{l})$ are independent of x . For T_1 there is a pressure component that depends linearly on x , but does not contribute to the drag.

The complete mean flow past one test rod is (cf. Howells 1974, equation (5.12))

$$\langle \mathbf{u} \rangle = \mathbf{U} + \mathbf{U}_1(\mathbf{r}),$$

with mean resistance force on fluid

$$\mathbf{R} = -\mu\alpha^2 \mathbf{U} + \mathbf{R}_1(\mathbf{r}).$$

These satisfy an equation that can be written, in re-normalized form,

$$-\nabla \langle p \rangle + \mu \nabla^2 \langle \mathbf{u} \rangle - \mu\alpha^2 \langle \mathbf{u} \rangle = -\mathbf{R} - \mu\alpha^2 \langle \mathbf{u} \rangle. \quad (5.1)$$

The stress distribution $T_1(x, \mathbf{a}; \mathbf{l})$ on the rod surface is such that the velocity vanishes there.

The solution can be expressed in terms of the three-dimensional Green's function (3.2) as

$$\langle \mathbf{u} \rangle = \mathbf{U} + \mathbf{U}_{T_1} + \mathbf{U}_{R_1},$$

where
$$\mathbf{U}_{T_1}(\mathbf{r}; \mathbf{l}) = -(8\pi\mu)^{-1} \int \oint T_1(x, \mathbf{a}; \mathbf{l}) \cdot \mathcal{I}(\mathbf{r} - x\mathbf{l} - \mathbf{a}) dL(\mathbf{a}) dx, \quad (5.2)$$

$$\mathbf{U}_{R_1}(\mathbf{r}; \mathbf{l}) = (8\pi\mu)^{-1} \int \{ \mathbf{R}_1(\mathbf{r}'; \mathbf{l}) + \mu\alpha^2 \mathbf{U}_1(\mathbf{r}'; \mathbf{l}) \} \cdot \mathcal{I}(\mathbf{r} - \mathbf{r}') d\mathbf{r}'. \quad (5.3)$$

Now apply the generalized Faxén's formula (3.6), with externally produced flow $\mathbf{u}_e = \mathbf{U} + \mathbf{U}_{R_1}$ (independent of x). The term \mathbf{U}_{T_1} represents the reflection in the cylinder of this externally produced flow. The mean drag per unit length is given by

$$\mathbf{f}_1^*(\mathbf{l}) = 4\pi\mu [\mathbf{C}_0^*(\mathbf{l}) \cdot \mathbf{U} + \{ \mathbf{C}_0(\mathbf{l}) + \mathbf{C}_2(\mathbf{l}) a^2 \nabla^2 \} \cdot \mathbf{U}_{R_1}(0)], \quad (5.4)$$

where the tensor coefficients depend on \mathbf{l} as shown in (3.6)–(3.7). $\mathbf{C}_0^*(\mathbf{l})$ includes the longitudinal pressure drag on finite rods. As pointed out at the end of §3, there is no longitudinal pressure drag contribution in the second and higher approximations.

The mean resistance force in the absence of test rods is given in terms of T_1 by

$$\mathbf{R} = - \int \left\{ \oint T_1(x, \mathbf{a}; \mathbf{l}) P(\boldsymbol{\sigma} - \mathbf{a}; \mathbf{l}) dL(\mathbf{a}) + \pi\mu\alpha^2 a^2 \mathbf{l} \cdot \mathbf{U} \right\} d\Omega(\mathbf{l}). \quad (5.5)$$

With the simplest form for the probability this is a constant, and from (1.2),

$$-\mathbf{R} = \mu\alpha^2 \mathbf{U} = \lambda/(4\pi) \int \mathbf{f}_1^*(\mathbf{l}) d\Omega(\mathbf{l}). \quad (5.6)$$

In the stage 1 approximation (denoted by a superscript 1), the hierarchy of equations is truncated by taking $\mathbf{R}_1 + \mu\alpha^2 \mathbf{U}_1$, and hence \mathbf{U}_{R_1} , as zero everywhere. This is equivalent to the statement that $\mathbf{R}_1^{(1)}$, $\mathbf{U}_1^{(1)}$ are related in the same way as \mathbf{R} and \mathbf{U} in uniform Darcy flow. The result is

$$\begin{aligned} \mathbf{U}_{T_1}^{(1)}(\mathbf{r}; \mathbf{l}) &= \mathbf{U}_1^{(1)}(\mathbf{r}; \mathbf{l}) \\ &= \begin{cases} -\mathbf{U} & \text{for } \sigma \leq a \\ 2\alpha^{-2}(\nabla\nabla - I\nabla^2) \cdot \{ \log(\alpha\sigma) \mathbf{C}_0(\mathbf{l}) + K_0(\alpha\sigma) \mathbf{C}_S(\mathbf{l}) \} \cdot \mathbf{U} & \text{for } \sigma > a \end{cases}. \end{aligned} \quad (5.7)$$

the disturbance flow due to a cylinder in Brinkman's medium (see §3).

It follows from (5.4) that $f_1^{(1)}(\mathbf{l}) = 4\pi\mu\mathbf{C}_0^*(\mathbf{l}) \cdot \mathbf{U}$. Substitution into (5.6) leads to the self-consistency equation (3.8).

5.3. Two test rods

The extension to two test rods (exact theory) proceeds in the same way as the extension from one test sphere to two in Howells (1974, §5). At this stage the contribution from end forces tends to zero in the limit of very long rods, hence we consider infinite cylinders. If the direction and position of the second rod are specified by the unit vector \mathbf{l}' and the position vector $\boldsymbol{\sigma}'$ perpendicular to \mathbf{l}' (figure 1), the mean flow at \mathbf{r} is written

$$\langle \mathbf{u} \rangle = \mathbf{U} + \mathbf{U}_1(\mathbf{r}; \mathbf{l}) + \mathbf{U}_1(\mathbf{r} - \boldsymbol{\sigma}'; \mathbf{l}') + \mathbf{U}_2(\mathbf{r}; 0, \mathbf{l}; \boldsymbol{\sigma}', \mathbf{l}'),$$

and similarly for \mathbf{R} . The mean surface stress discontinuity at $\boldsymbol{\sigma}' + x'\mathbf{l}' + \mathbf{a}'$ on rod 2 ($|\mathbf{a}'| = a$, $\mathbf{a}' \cdot \mathbf{l}' = 0$) is

$$\mathbf{T}_1(x', \mathbf{a}'; \mathbf{l}') + \mathbf{T}_2(x', \mathbf{a}'; \boldsymbol{\sigma}', \mathbf{l}'; 0, \mathbf{l}),$$

and there is a corresponding expression for the stress at $x\mathbf{l} + \mathbf{a}$ on rod 1.

5.4. Preliminary result

The extra force per unit length at x on rod 1, due to the presence of rod 2, is

$$\mathbf{f}_2(x; 0, \mathbf{l}; \boldsymbol{\sigma}', \mathbf{l}') = \oint \mathbf{T}_2(x, \mathbf{a}; 0, \mathbf{l}; \boldsymbol{\sigma}', \mathbf{l}') dL(\mathbf{a}),$$

which is associated with the extra velocity field at the first axis due to the presence of the second rod:

$$\mathbf{U}_1(\mathbf{r} - \boldsymbol{\sigma}'; \mathbf{l}') + \mathbf{U}_2(\mathbf{r}; 0, \mathbf{l}; \boldsymbol{\sigma}', \mathbf{l}').$$

For a drag calculation, this velocity field must be separated into the part resulting from forces external to the first rod, and that produced by the extra stress \mathbf{T}_2 on the first rod. The externally produced part is

$$\begin{aligned} \mathbf{u}_e &= \mathbf{U}_1(\mathbf{r} - \boldsymbol{\sigma}'; \mathbf{l}') + \mathbf{U}_{R2}(\mathbf{r}; 0, \mathbf{l}; \boldsymbol{\sigma}', \mathbf{l}') \\ &\quad - (8\pi\mu)^{-1} \int \oint \mathbf{T}_2(x', \mathbf{a}'; \boldsymbol{\sigma}', \mathbf{l}'; 0, \mathbf{l}) \cdot \mathcal{I}(\mathbf{r} - \boldsymbol{\sigma}' - x'\mathbf{l}' - \mathbf{a}') dL(\mathbf{a}') dx'. \end{aligned}$$

Here \mathbf{U}_{R2} is defined by analogy with equation (5.3). In the truncation for stage 2 it is taken to be zero.

The integral of \mathbf{f}_2 over all x (i.e. the total additional force on rod 1 due to the presence of rod 2) is finite. With the above choice of \mathbf{u}_e , it is shown in Appendix A, equations (A 11) and (A 12), that this can be expressed as

$$\begin{aligned} &\int_{-\infty}^{\infty} \mathbf{f}_2(x; 0, \mathbf{l}; \boldsymbol{\sigma}', \mathbf{l}') dx \\ &= 4\pi\mu \int_{-\infty}^{\infty} \{ \mathbf{C}_0(\mathbf{l}) + \mathbf{C}_2(\mathbf{l}) a^2 \nabla^2 \} \cdot \{ \mathbf{U}_1(x\mathbf{l} + \boldsymbol{\sigma} - \boldsymbol{\sigma}'; \mathbf{l}') + \mathbf{U}_{R2}(x\mathbf{l} + \boldsymbol{\sigma}; 0, \mathbf{l}; \boldsymbol{\sigma}', \mathbf{l}') \} dx \Big|_{\sigma=0} \\ &\quad - \frac{1}{2} \{ \mathbf{C}_0(\mathbf{l}) + \mathbf{C}_2(\mathbf{l}) a^2 \nabla^2 \} \cdot \int_{-\infty}^{\infty} dx \int_{-\infty}^{\infty} dx' \\ &\quad \times \oint \mathbf{T}_2(x', \mathbf{a}'; \boldsymbol{\sigma}', \mathbf{l}'; 0, \mathbf{l}) \cdot \mathcal{I}(\boldsymbol{\sigma} + x\mathbf{l} - \boldsymbol{\sigma}' - x'\mathbf{l}' - \mathbf{a}') dL(\mathbf{a}') \Big|_{\sigma=0}. \end{aligned} \tag{5.8}$$

5.5. Mean drag on one test rod at stage 2

To evaluate expression (5.4) for the mean drag on one test rod, the additional mean resistance force at r due to the presence of this rod is to be expressed by means of probability integrals of T_1 , T_2 taken over all positions of a second rod (compare Howells 1974, equation (5.7)):

$$\begin{aligned} R_1(x'l + \sigma'; l) = & - \int \oint T_1(x', a'; l') \{P(\sigma' - a', l' | 0, l) - \lambda/4\pi\} dL(a') d\Omega(l') \\ & - \int \oint T_2(x', a'; \sigma' - a', l'; 0, l) P(\sigma' - a', l' | 0, l) dL(a') d\Omega(l'). \end{aligned}$$

Substitution into (5.3), and a change of variable in the integrals, leads to

$$\begin{aligned} U_{R1}(r; l) = & \int \int U_{T1}(r - \sigma'; l') \{P(\sigma', l' | 0, l) - \lambda/4\pi\} dA(\sigma') d\Omega(l') \\ & + \alpha^2/(8\pi) \int U_1(r'; l) \cdot \mathcal{J}(r - r') dr' \\ & - (8\pi\mu)^{-1} \int d\Omega(l') \int P(\sigma', l' | 0, l) dA(\sigma') \\ & \times \int_{-\infty}^{\infty} \oint T_2(x', a'; \sigma', l'; 0, l) \cdot \mathcal{J}(r - \sigma' - x'l - a') dL(a') dx'. \quad (5.9) \end{aligned}$$

In these integrals the $dA(\sigma')$ integration is taken over the whole plane normal to l' . For the third term in (5.9), it is expressed as a repeated integral by means of the transformation $dA(\sigma') = \sin \theta dx dh$, where x is the position on rod 1 of the foot of the common normal, and h is its length (see (2.4)). Given statistical homogeneity, the probability density can be taken outside the x -integration thus introduced.

The operator $\{\mathbf{C}_0(l) + \mathbf{C}_2(l) a^2 \nabla^2\}$ is now applied to U_{R1} , so as to evaluate the expression (5.4), and the result (5.8) is used to eliminate the integral involving T_2 . It is found that

$$(4\pi\mu)^{-1} f_1(l) = \mathbf{C}_0(l) \cdot U + W_1 + W_2 + W_3 + W_S,$$

where

$$W_1 = \{\mathbf{C}_0(l) + \mathbf{C}_2(l) a^2 \nabla^2\} \cdot \int \int U_{T1}(r - \sigma'; l') \{P(\sigma', l' | 0, l) - \lambda/4\pi\} dA(\sigma') d\Omega(l') |_{r=0},$$

$$W_2 = \frac{\alpha^2}{8\pi} \{\mathbf{C}_0(l) + \mathbf{C}_2(l) a^2 \nabla^2\} \cdot \int U_1(r'; l) \cdot \mathcal{J}(r - r') dr' |_{r=0},$$

$$\begin{aligned} W_3 = & \int \sin \theta d\Omega(l') \int_0^\infty P(\sigma', l' | 0, l) dh \\ & \times \int_{-\infty}^\infty \{(4\pi\mu)^{-1} f_2(x; 0, l; \sigma', l') - \{\mathbf{C}_0(l) + \mathbf{C}_2(l) a^2 \nabla^2\} \cdot U_1(xl + \sigma - \sigma'; l') |_{\sigma=0}\} dx, \end{aligned}$$

$$\begin{aligned} W_S = & - \int \sin \theta d\Omega(l') \int_0^\infty P(\sigma', l' | 0, l) dh \\ & \times \int_{-\infty}^\infty \{\mathbf{C}_0(l) + \mathbf{C}_2(l) a^2 \nabla^2\} \cdot U_{R2}(xl + \sigma; 0, l; \sigma', l') |_{\sigma=0} dx. \end{aligned}$$

5.6. Stage 2 approximation

As has been pointed out, the truncation now involves omission of U_{R2} and hence of W_S . In the integrals for W_1 , W_2 , W_3 the first approximations are used for the velocity fields: $U_1^{(1)}(\mathbf{r}; I)$, $U_{T1}^{(1)}(\mathbf{r}; I)$, and these are equal (see (5.7)). The first two integrals can be evaluated algebraically (refer to (2.5) for $P(\boldsymbol{\sigma}', I' | 0, I)$):

$$\begin{aligned} W_1 &= \{\mathbf{C}_0(I) + \mathbf{C}_2(I) a^2 \nabla^2\} \cdot \int d\Omega(I') \int U_1^{(1)}(\mathbf{r} - \boldsymbol{\sigma}'; I') \{P(\boldsymbol{\sigma}', I' | 0, I) - \lambda/4\pi\} dA(\boldsymbol{\sigma}')|_{r=0} \\ &= c \left[\frac{4}{3}(\alpha a)^{-2} \{C_T^2 - C_S^2(1 + 2\alpha a) e^{-2\alpha a}\} (I + \frac{1}{4}II) - \frac{5}{6}C_T II \right] \cdot U, \end{aligned} \quad (5.10)$$

$$\begin{aligned} W_2 &= \frac{\alpha^2}{8\pi} \{\mathbf{C}_0(I) + \mathbf{C}_2(I) a^2 \nabla^2\} \cdot \int \mathcal{J}(\mathbf{r} - \mathbf{r}') \cdot U_1^{(1)}(\mathbf{r}'; I) d\mathbf{r}'|_{r=0} \\ &= \{-2C_L^2(I - \frac{1}{2}II) + \frac{1}{4}\alpha^2 a^2 II\} \cdot U. \end{aligned} \quad (5.11)$$

In W_3 the first approximation to $f_2(x; 0, I; \boldsymbol{\sigma}', I')$ will be given in terms of Ψ , the Fourier transform of the surface stress, obtained from the calculations described in the Appendices. The integral of this over all x is shown there, (A 12), to be given by $4\pi^2\mu\Psi_0''(0)$ (sum of first and higher reflections). The integral of the subtracted term $\{\mathbf{C}_0(I) + \mathbf{C}_2(I) a^2 \nabla^2\} \cdot U_1(xI + \boldsymbol{\sigma} - \boldsymbol{\sigma}'; I')|_{\sigma=0}$ is $(4\pi\mu)^{-1}$ times the total force due to the first reflection, and hence

$$\int_{-\infty}^{\infty} \{(4\pi\mu)^{-1} f_2(x; 0, I; \boldsymbol{\sigma}', I') - \{\mathbf{C}_0(I) + \mathbf{C}_2(I) a^2 \nabla^2\} \cdot U_1(xI + \boldsymbol{\sigma} - \boldsymbol{\sigma}'; I')|_{\sigma=0}\} dx$$

is given to the first approximation by $\pi\Psi_0''(0)$, the sum of contributions to $\pi\Psi_0(0)$ from second and higher reflections. Hence

$$\begin{aligned} W_3 &= \int_0^{\infty} P(\boldsymbol{\sigma}', I' | 0, I) dh \int_0^{\pi} \sin^2 \theta d\theta \int_0^{2\pi} \pi\Psi_0''(0) d\phi \\ &= \frac{1}{4}\lambda \int_{2a}^{\infty} \{1 + 2a\delta(h - 2a)\} dh \int_{-\pi}^{\pi} \sin^2 \theta d\theta \int_0^{2\pi} \Psi_0''(0) d\phi \\ &= cQ_1(\alpha a) II \cdot U + cQ_2(\alpha a) (I - II) \cdot U, \end{aligned} \quad (5.12)$$

where Q_1 , Q_2 are defined at the end of Appendix B. Their calculation is explained, and approximate values are given there.

Of these integrals, W_1 represents the effect of the ‘excluded volume’ around any fibre, W_2 the re-normalizing term $-\mu\alpha^2 U_1(\mathbf{r}'; I)$ that appears on the right-hand side of equation (5.1), W_3 the contribution of the two-cylinder interactions to the drag (its leading term, the second reflection, is in fact nearly cancelled out by W_2), and W_S the higher-order contributions that are omitted at stage 2.

Note the effect in W_1 and W_3 of the accumulated probability at $h = 2a$. In the former, (5.10), the effect is represented simply by the term $2\alpha a$ in the bracket multiplying $\exp(-2\alpha a)$. As $\alpha a \rightarrow 0$, W_1 behaves like $(\log \alpha a)^{-2}$ when the accumulated probability term is included, but like $(\alpha a)^{-1} (\log \alpha a)^{-2}$ when it is not. In W_3 , it can be seen from (B 7) that the effect is expressed in the term $2S_k$ added to R_k which represents integrals over h .

6. Self-consistency equation and stage 2 results for drag

Substitution of the stage 2 approximation

$$(4\pi\mu)^{-1} f_1^{(2)}(I) = \mathbf{C}_0^*(I) \cdot U + W_1 + W_2 + W_3 \quad (6.1)$$

into (5.6) leads to

$$c/(4\pi) \int \{\mathbf{C}_0^*(\mathbf{l}) \cdot \mathbf{U} + \mathbf{W}_1 + \mathbf{W}_2 + \mathbf{W}_3\} d\Omega(\mathbf{l}) = \frac{1}{4}\alpha^2 a^2 \mathbf{U}.$$

From this the self-consistency equation can be written

$$\frac{1}{4}\alpha^2 a^2 = cG(\alpha a) + c^2 H(\alpha a) \quad (6.2)$$

in terms of functions G , H such that

$$\int \{\mathbf{C}_0^*(\mathbf{l}) \cdot \mathbf{U} + \mathbf{W}_2\} d\Omega(\mathbf{l}) = 4\pi G(\alpha a) \mathbf{U},$$

$$\int \{\mathbf{W}_1 + \mathbf{W}_3\} d\Omega(\mathbf{l}) = 4\pi c H(\alpha a) \mathbf{U}.$$

Equations (3.7)–(3.8) and (5.10)–(5.12) show that these notations are consistent and that

$$G(\alpha a) = \frac{5}{3}C_L(1 - C_L) + \frac{1}{2}\alpha^2 a^2,$$

$$H(\alpha a) = \frac{13}{9}(\alpha a)^{-2} \{C_T^2 - C_S^2(1 + 2\alpha a) e^{-2\alpha a}\} - \frac{5}{18}C_T + \frac{1}{3}Q_1(\alpha a) + \frac{2}{3}Q_2(\alpha a),$$

where as in §3,

$$C_S = 1/K_0(\alpha a), \quad C_L = \frac{1}{2}\alpha a K_1(\alpha a)/K_0(\alpha a),$$

$$C_T = \frac{1}{2}\alpha^2 a^2 K_2(\alpha a)/K_0(\alpha a) = 2C_L + \frac{1}{2}\alpha^2 a^2.$$

For longitudinal/transverse flow through arrays of *parallel* rods, the corresponding functions are

Longitudinal

$$W_1 = 2c(\alpha a)^{-2} \{C_T C_L - \alpha a K_1(2\alpha a) C_S^2\} \mathbf{U},$$

$$W_2 = (-C_L^2 + \frac{1}{4}\alpha^2 a^2) \mathbf{U}, \quad W_3 = cQ_l(\alpha a) \mathbf{U},$$

$$G(\alpha a) = C_L(1 - C_L) + \frac{1}{2}\alpha^2 a^2, \quad H(\alpha a) = 2(\alpha a)^{-2} \{C_T C_L - \alpha a K_1(2\alpha a) C_S^2\} + Q_l(\alpha a);$$

Transverse

$$W_1 = 2c(\alpha a)^{-2} \{C_T^2 - 2\alpha a K_1(2\alpha a) C_S^2\} \mathbf{U},$$

$$W_2 = -2C_L^2 \mathbf{U}, \quad W_3 = cQ_t(\alpha a) \mathbf{U},$$

$$G(\alpha a) = 2C_L(1 - C_L) + \frac{1}{2}\alpha^2 a^2, \quad H(\alpha a) = 2(\alpha a)^{-2} \{C_T^2 - 2\alpha a K_1(2\alpha a) C_S^2\} + Q_t(\alpha a).$$

Here

$$Q_l(\alpha a) = 2a^{-2} \int_{2a}^{\infty} d_{11} h dh, \quad Q_t(\alpha a) = a^{-2} \int_{2a}^{\infty} (d_{22} + d_{33}) h dh,$$

where the d_{ii} are drag coefficients, relating to the sum of second and higher reflections, for a pair of parallel rods a distance h apart: d_{11} for longitudinal flow, d_{22} for transverse flow at right angles to the plane of the two rods, d_{33} for transverse flow in the plane of the rods.

From equation (6.2) the volume fraction c is found as a function of the parameter αa . Equation (6.1), together with (5.10)–(5.12), provides the results for transverse and longitudinal drag at the stage 2 approximation.

All these results for very long straight filaments, at both first and second

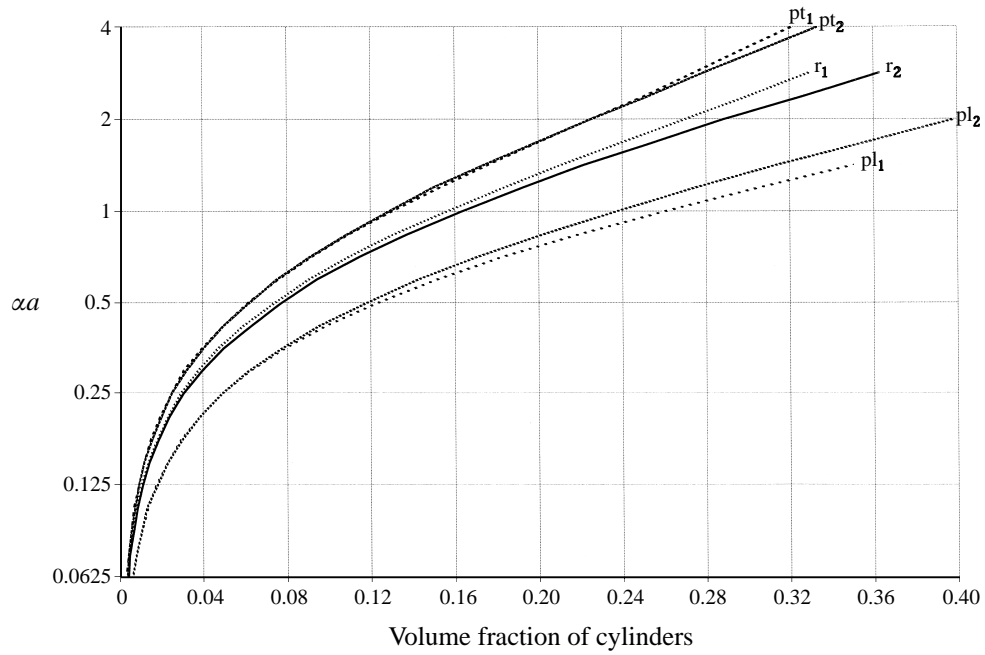


FIGURE 2. Graphs of parameter αa against volume fraction of cylinders. pl, arrays of parallel rods with longitudinal flow; pt, arrays of parallel rods with transverse flow; r, arrays of randomly oriented rods. Suffices 1, 2 denote stage of approximation.

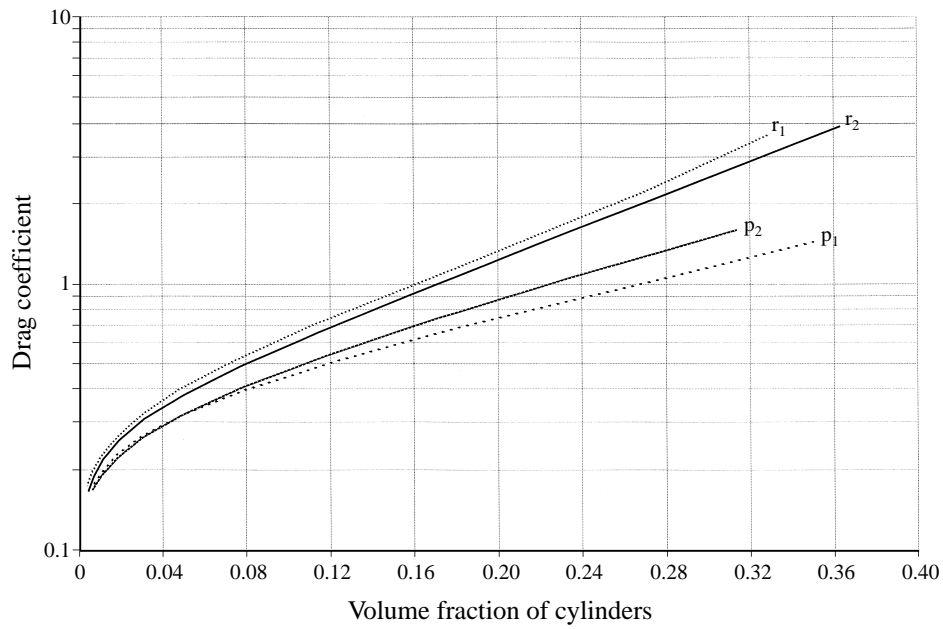


FIGURE 3. Graphs of longitudinal drag coefficient against volume fraction of cylinders. p, arrays of parallel rods; r, arrays of randomly oriented rods. Suffices 1, 2 denote stage of approximation.

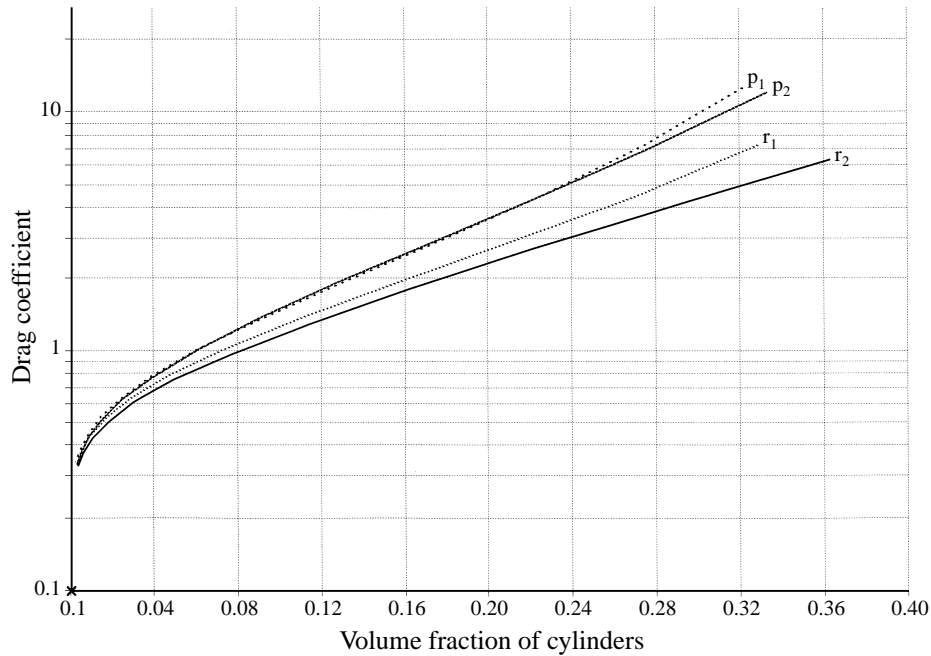


FIGURE 4. Graphs of transverse drag coefficient against volume fraction of cylinders. p , arrays of parallel rods; r , arrays of randomly oriented rods. Suffixes 1, 2 denote stage of approximation.

approximations, are shown in figures 2–4, converted so as to make c the independent variable. Figure 2 gives the parameter αa as a function of c , figure 3 the longitudinal drag, and figure 4 the transverse drag. In each case the results for arrays of parallel rods are included for comparison. Clearly the graphs are extended far beyond the range of applicability of the assumptions about sparse arrays. See the conclusion for comments about the comparison between the first and second approximation.

7. Comparison with experimental results

Spielman & Goren (1968) compare their drag predictions for a bed of fibres, randomly oriented at right angles to the direction of flow, with an empirical curve of Davies (1952). In the middle range of fibre volume fraction, the agreement is good. At lower values of the volume fraction the empirical curve appears to tend to a constant value, instead of decreasing without limit as predicted theoretically: this is presumably the effect of finite Reynolds number found by Kaneda (1986).

For volume fractions greater than 0.06, the empirical curve falls below the theoretical one. At $c = 0.1$ the difference rises to 10% and at 0.2 to 25%. Calculations that include the effect of anisotropy, as explained in §3, agree much better with the empirical curve. (The correction for two-cylinder interactions becomes comparable to the effect of anisotropy at volume fractions approaching 0.3.) Thus the claim made by the authors that the effect of anisotropic resistance will be small is valid only for the lower values of volume fraction.

Evans *et al.* (1994) present experimental work on polymer conformation during flow through a fixed fibre bed, where the fibres are randomly placed in each of two orthogonal directions normal to the flow. For volume fraction 0.0247 and fibres of

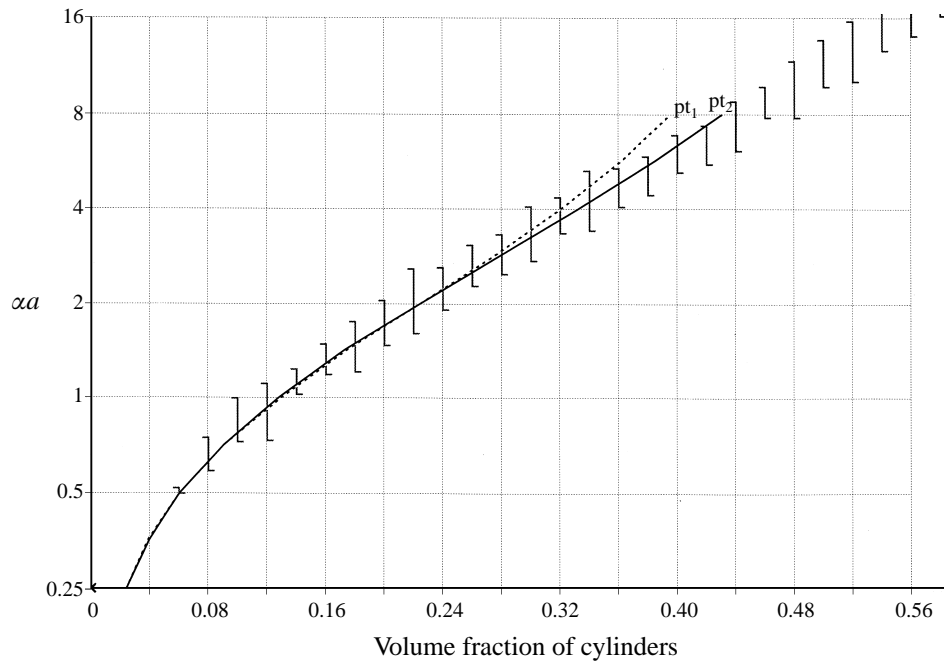


FIGURE 5. Comparison of numerical experiment of Ghaddar (1995) on transverse flow through random arrays of parallel cylinders, with theoretical predictions. Parameters αa as function of volume fraction. One standard deviation range of confidence for numerical experiment, vertical bars; theoretical predictions: ---- pt₁, first approximation; — pt₂, second approximation.

diameter 0.0203 cm, they give an accurate drag measurement leading to a ‘pore size’ (shielding length) of 0.0421 cm, as against their theoretical value of 0.0486 cm. It seems likely that the difference is largely due to their approximating the modified Bessel function by the logarithmic leading term. The exact method of Spielman & Goren (1968) and of the present paper, for transverse flow through parallel arrays, gives a first approximation pore size of 0.0403 cm. Allowance for the effect of anisotropy as described in §3 raises this to 0.0410 cm. The second approximation has not been worked out for this configuration, but an estimate by analogy with transverse flow through parallel arrays suggests a drag reduction of about 4%, bringing the pore size to 0.0418 cm.

Ghaddar (1995) employed a Monte Carlo approach to compute the transverse permeability of random arrays of parallel fibres. His table III gives results that can be directly compared with the parallel fibre theory. Ghaddar compares three of his data points with the results given by Howells (1974). His remarks, on the stabilizing effect of incorporating the averaged effect of a second cylinder, are supported by consideration of figure 5. This shows upper and lower estimates of the parameter αa , from his one-standard-deviation confidence limits for permeability, with the first and second approximation curves from the present paper.

Experimental work on beds of fibres randomly orientated in three dimensions is evidently more difficult, and so far data have not been found to compare with the theory.

8. Conclusions

The successive approximation approach to the problem of flow through a fixed bed, developed from the averaged equation method with re-normalization, is based on quite simple equations. First, there are equations (3.1) for the Brinkman effective medium, together with an equation for self-consistency, such as (5.6). These lead to first approximations that are good for c up to 0.05, and fair up to even 0.2. Factors such as finite length and curvature can be allowed for by ordinary drag calculations for the Brinkman medium.

Secondly, the re-normalized equation (5.1) leads to the stage 2 expression (6.1), with W_1 , W_2 , W_3 given in (5.10), (5.11), (5.12). As pointed out, these three expressions have clear physical meanings, though the drag calculation for the third involves some extensive computation in the case of randomly oriented rods. The results to stage 2, and comparison with experiments, give further confidence in the approach.

8.1. Formal order of magnitude of the error for asymptotically small volume fraction

For the regime of asymptotically small c , it was pointed out in the introduction that expansions for the drag coefficient in terms of c have not just negative powers of $\log 1/c$ but also repeated logarithms, which is not a very useful kind of series.

The implicit formulation of Howells (1974) (see (1.1)) expresses $\log 1/c$ as a series beginning with the first power of the divisor M (reciprocal of transverse drag coefficient), then its logarithm plus a constant, and then all negative powers. Thus if $2M = \log 1/c$ is taken as the basic approximation, the error is of order $\log \log 1/c$. It is surely preferable to use the implicit equation $2M - \log M + 2\gamma = \log m/c$ (m is 1, 2, $\frac{6}{5}$, ..., depending on the geometry of the fibre array) to define the first approximation. Now the first term neglected in the expression for $\log 1/c$ is of order M^{-1} . At the second approximation (two rods), the first term neglected is of order M^{-2} , and so on.

8.2. Behaviour of the approximation process at practical values of volume fraction

Consider now a regime for which terms in c are significant. It turns out that the value of M may be too small for expansions in negative powers of M to be useful. For the two-rod calculations in §§5 and 6, the drag terms were evaluated numerically for a range of values of αa corresponding to this regime. Then, with parallel arrays, for transverse flow the change produced by the second-order theory is less than 4% up to $c = 0.2$, and for longitudinal flow the change is less than 4% up to $c = 0.075$, and 8% at 0.1. With random arrays, whether for transverse or longitudinal flow, the change is less than 6% up to $c = 0.03$, and less than 10% up to $c = 0.2$.

Given the fair degree of closeness between first and second approximations up to volume fractions of 0.2, it may be of interest to set out the behaviour of the present theory at the highest values of c :

Parallel arrays, near to close packing. On physical grounds, transverse flow is blocked at close packing, $c = 0.907$. Use of the asymptotic forms for the modified Bessel functions leads to results from the present theory for the dependence of αa , when it is large, on c : first-order theory $\alpha a = 1/(0.5 - c)$; second-order $\alpha a = 2.673c/(0.604 - c)$. Longitudinal flow is not quite blocked at close packing, but αa should be around 60. From first-order theory $\alpha a = 2/(1 - c) \approx 21.5$ at close packing; from second-order theory $\alpha a = 3c/(1 - c) \approx 29.2$ at close packing.

Random arrays, densely packed. At the closest packing $c = 0.680$, and from the first-order theory $\alpha a = 1.2/(0.6 - c)$. The calculation has not been carried out for the second-order theory. In all these cases note that $C_T = 2C_L^* \approx \frac{1}{2}\alpha^2 a^2 + \alpha a$.

The author acknowledges his indebtedness to the Department of Mathematics at the University of Queensland, for his appointment as Honorary Research Adviser during the period when this paper was being brought to completion. At an earlier stage the computing facilities at the Department of Mathematics in the University of Adelaide, where the author was tutor, were employed.

Appendix A: Fourier transforms of flow fields

Flows in the Brinkman's medium can be expressed as Fourier transforms in cylindrical polar coordinates (x, σ, ϕ) (with notation $\kappa_\alpha = (\kappa^2 + \alpha^2)^{1/2}$):

$$(1 - \alpha^{-2} \nabla^2) \mathbf{u} = \int_{-\infty}^{\infty} \sum_{n=-\infty}^{\infty} \alpha^{-2} \mathbf{H}_n(\kappa) \cdot (\nabla \nabla - I \nabla^2) I_n(|\kappa| \sigma) e^{i\kappa x + in\phi} d\kappa, \quad (\text{A } 1)$$

$$\alpha^{-2} \nabla^2 \mathbf{u} = - \int_{-\infty}^{\infty} \sum_{n=-\infty}^{\infty} \alpha^{-2} \mathbf{\Omega}_n(\kappa) \cdot (\nabla \nabla - I \nabla^2) I_n(\kappa_\alpha \sigma) e^{i\kappa x + in\phi} d\kappa. \quad (\text{A } 2)$$

The velocity field \mathbf{u} is clearly the sum of the two expressions (A 1) and (A 2). But it is convenient to treat them separately: (A 1) is an irrotational flow driven by the pressure field against Darcy resistance, and (A 2) is a rotational flow governed by viscous forces.

For the flow due to a shielded Stokeslet \mathcal{S} at the point $(x, \sigma, \phi) = (0, h, 0)$, which is given by the Green's function (3.2), the Fourier transforms that appear above are

$$\mathbf{H}_n(\kappa) = \mathcal{S} K_n(|\kappa| h), \quad \mathbf{\Omega}_n(\kappa) = \mathcal{S} K_n(\kappa_\alpha h). \quad (\text{A } 3)$$

These expressions display the typical behaviours, as $\kappa \rightarrow 0, \infty$, of the Fourier transforms that arise in this section.

A.1. Expansion in cylindrical coordinates of the flow due to an inclined cylinder

The notation is mostly as in §2, figure 1: the axes have directions \mathbf{l}, \mathbf{l}' , inclined at angle θ , and the shortest distance between them is h . But now x, x' are measured along the respective rod axes from O, O' , which are the ends of the common normal (see figure 6). Azimuthal angles ϕ, ϕ' are measured from \mathbf{n}, \mathbf{n}' .

A surface stress distribution $\mathbf{P}(x', \phi')$, acting on the fluid over a cylinder of radius a about the second axis, is expressed as a Fourier transform:

$$\mathbf{P}(x', \phi') = \mu a^{-1} \int_{-\infty}^{\infty} \sum_{n=-\infty}^{\infty} \mathbf{\Phi}_n(\kappa') e^{i\kappa' x' + in\phi'} d\kappa'.$$

The resulting flow can be expanded in coordinates (x, σ, ϕ) about the first axis, using the equations (A 1), (A 2) with

$$\left. \begin{aligned} \mathbf{H}_j(\kappa) &= |2 \sin \theta|^{-1} \int_{-\infty}^{\infty} \sum_{n=-\infty}^{\infty} \left(\frac{q - \kappa'''}{\kappa} \right)^j \left(\frac{q - \kappa''}{\kappa'} \right)^n e^{-qh} I_n(|\kappa'| a) \mathbf{\Phi}_n(\kappa') \frac{d\kappa'}{q}, \\ \mathbf{\Omega}_j(\kappa) &= |2 \sin \theta|^{-1} \int_{-\infty}^{\infty} \sum_{n=-\infty}^{\infty} \left(\frac{q_\alpha - \kappa'''}{\kappa_\alpha} \right)^j \left(\frac{q_\alpha - \kappa''}{\kappa'_\alpha} \right)^n e^{-q_\alpha h} I_n(\kappa'_\alpha a) \mathbf{\Phi}_n(\kappa') \frac{d\kappa'}{q_\alpha}, \end{aligned} \right\} \quad (\text{A } 4)$$

and the notation

$$\left. \begin{aligned} \kappa'' &= (\kappa - \kappa' \cos \theta) / \sin \theta, & \kappa_\alpha &= (\kappa^2 + \alpha^2)^{1/2}, \\ \kappa''' &= (\kappa' - \kappa \cos \theta) / \sin \theta, & \kappa'_\alpha &= (\kappa'^2 + \alpha^2)^{1/2}, \\ q &= (\kappa^2 + \kappa'^2 - 2\kappa\kappa' \cos \theta)^{1/2} / |\sin \theta|, & q_\alpha &= (q^2 + \alpha^2)^{1/2}. \end{aligned} \right\} \quad (\text{A } 5)$$

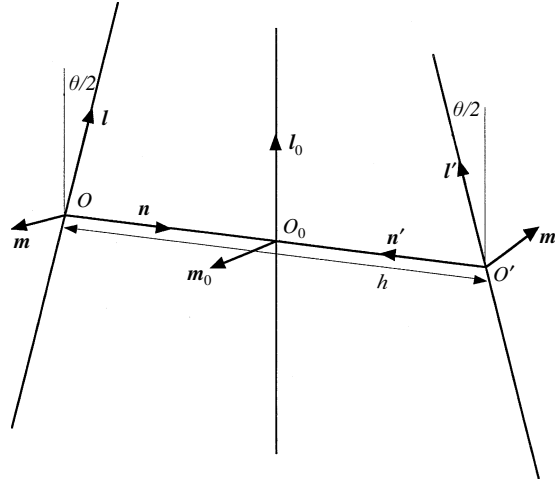


FIGURE 6. Axes of symmetry for inclined cylinders.

Equations (A 4) yield $\Pi_j(\kappa)$, $\Omega_j(\kappa)$ that behave similarly to the forms given in (A 3), namely regular functions of real κ , except that as $\kappa \rightarrow 0$, $\Pi_j(\kappa)$ is $O(\kappa^{-|j|})$ for $j \neq 0$ and $O(\log \kappa)$ for $j = 0$. They are exponentially small for large κ .

For parallel axes, $\theta = 0$, and the transformation simplifies to

$$\begin{aligned}\Pi_j(\kappa) &= \sum_{n=-\infty}^{\infty} K_{j-n}(|\kappa|h) I_n(\kappa a) \Phi_n(\kappa), \\ \Omega_j(\kappa) &= \sum_{n=-\infty}^{\infty} K_{j-n}(\kappa_\alpha h) I_n(\kappa_\alpha a) \Phi_n(\kappa).\end{aligned}$$

A.2. Analogues of Faxén's formulae

The next step is to find the surface force distribution on a rigid cylinder having its axis in direction I through O , as a result of this externally produced flow, given by (A 1)–(A 2), (A 4)–(A 5) and denoted $\mathbf{u}_e(x, \sigma, \phi)$.

Let the unknown surface force per unit area, acting on this cylinder from the fluid, be written as a Fourier transform

$$\mathcal{Q}(x, \phi) = \mu a^{-1} \int_{-\infty}^{\infty} \sum_{n=-\infty}^{\infty} \Psi_n(\kappa) e^{i\kappa x + in\phi} d\kappa. \quad (\text{A } 6)$$

Then following the method of Howells (1974, p. 456), the fact that the cylinder is rigid is expressed by the equations (as before $\kappa_\alpha = (\kappa^2 + \alpha^2)^{1/2}$)

$$\begin{aligned}\sum_{n=-\infty}^{\infty} \{K_n(|\kappa|a) \Psi_n(\kappa) - \Pi_n(\kappa)\} \cdot (\nabla \nabla - I \nabla^2) I_n(|\kappa| \sigma) e^{i\kappa x + in\phi} &= 0, \\ \sum_{n=-\infty}^{\infty} \{K_n(\kappa_\alpha a) \Psi_n(\kappa) - \Omega_n(\kappa)\} \cdot (\nabla \nabla - I \nabla^2) I_n(\kappa_\alpha \sigma) e^{i\kappa x + in\phi} &= 0,\end{aligned}$$

which hold for all κ , and all points within the cylinder. After the differential operations have been carried out, scalar components are taken, and Fourier components in the angle ϕ . Then those equations are selected that involve the adjacent suffices $j-1$, j , $j+1$: six equations that reduce to three independent ones:

$$\begin{aligned}K_{j+1}(\kappa a) (\mathbf{m} + i\mathbf{n}) \cdot \Psi_{j+1} - K_{j-1}(\kappa a) (\mathbf{m} - i\mathbf{n}) \cdot \Psi_{j-1} - (\kappa/|\kappa|) 2K_j(\kappa a) I \cdot \Psi_j \\ = (\mathbf{m} + i\mathbf{n}) \cdot \Pi_{j+1} - (\mathbf{m} - i\mathbf{n}) \cdot \Pi_{j-1} - (\kappa/|\kappa|) 2I \cdot \Pi_j,\end{aligned}$$

and

$$\begin{aligned} (\kappa_\alpha/\kappa) \mathbf{l} \cdot \{K_j(\kappa_\alpha a) \boldsymbol{\Psi}_j - \boldsymbol{\Omega}_j\} &= -(\mathbf{m} - \mathbf{in}) \cdot \{K_{j-1}(\kappa_\alpha a) \boldsymbol{\Psi}_{j-1} - \boldsymbol{\Omega}_{j-1}\} \\ &= (\mathbf{m} + \mathbf{in}) \cdot \{K_{j+1}(\kappa_\alpha a) \boldsymbol{\Psi}_{j+1} - \boldsymbol{\Omega}_{j+1}\}. \end{aligned}$$

The consistent, unique solution for the $\boldsymbol{\Psi}_j(\kappa)$ can now be found in terms of the known sequences $\boldsymbol{\Pi}_j(\kappa)$, $\boldsymbol{\Omega}_j(\kappa)$. Define the sequence of scalar functions

$$N_j(\kappa) = \frac{(\mathbf{m} - \mathbf{in}) \cdot (\boldsymbol{\Pi}_{j-1} - M_{j-1} \boldsymbol{\Omega}_{j-1}) - (\mathbf{m} + \mathbf{in}) \cdot (\boldsymbol{\Pi}_{j+1} - M_{j+1} \boldsymbol{\Omega}_{j+1}) + 2\mathbf{l} \cdot (\boldsymbol{\Pi}_j - M_j \boldsymbol{\Omega}_j)}{M_{j+1} + M_{j-1} - 2|\kappa/\kappa_\alpha| M_j}, \quad (\text{A } 7)$$

where

$$M_j(\kappa) = K_j(|\kappa| a) / K_j(\kappa_\alpha a); \quad (\text{A } 8)$$

then the $\boldsymbol{\Psi}_j$ are given by

$$K_j(\kappa_\alpha a) \boldsymbol{\Psi}_j(\kappa) - \boldsymbol{\Omega}_j(\kappa) = \frac{1}{2}(\mathbf{m} + \mathbf{in}) N_{j+1}(\kappa) - \frac{1}{2}(\mathbf{m} - \mathbf{in}) N_{j-1}(\kappa) - \mathbf{l} N_j(\kappa) \kappa / \kappa_\alpha. \quad (\text{A } 9)$$

The resultant drag force on the circumference of the cylinder at x , per unit length along the cylinder, is

$$\mathbf{f}(x) = 2\pi\mu \int_{-\infty}^{\infty} \boldsymbol{\Psi}_0(\kappa) e^{i\kappa x} d\kappa. \quad (\text{A } 10)$$

And

$$\int_{-\infty}^{\infty} \mathbf{f}(x) dx = 4\pi^2 \mu \boldsymbol{\Psi}_0(0), \quad (\text{A } 11)$$

when it exists, is the total drag force on the whole cylinder.

Letting κ tend to zero in (A 7)–(A 9), and using (A 1), (A 2) to interpret the resulting limits in terms of the externally produced velocity field, we find for the total drag (see (3.5)–(3.7))

$$4\pi^2 \mu \boldsymbol{\Psi}_0(0) = \int_{-\infty}^{\infty} 4\pi\mu \{ \mathbf{C}_0(\mathbf{l}) + \mathbf{C}_2(\mathbf{l}) a^2 \nabla^2 \} \cdot \mathbf{u}_e(x, 0, \phi) dx. \quad (\text{A } 12)$$

In the case where the velocity field \mathbf{u}_e is independent of x ,

$$\text{write} \quad (1 - \alpha^{-2} \nabla^2) \mathbf{u}_e = \sum_{k=-\infty}^{\infty} V_k(\sigma/a)^{|k|} e^{ik\phi} \quad (\mathbf{l} \cdot V_k = 0 \quad \text{for } k \neq 0) \quad (\text{A } 13)$$

and

$$\alpha^{-2} \nabla^2 \mathbf{u}_e = \sum_{k=-\infty}^{\infty} W_k I_k(\alpha\sigma) e^{ik\phi}.$$

Then

$$\begin{aligned} K_0(\alpha a) \boldsymbol{\Psi}_0(\kappa) &= (2\mathbf{l} - \mathbf{l}) \cdot \left\{ \frac{1}{2} \alpha^2 a^2 K_2(\alpha a) V_0 + W_0 \right\} \delta(\kappa) - \frac{1}{2} \alpha^2 a^2 K_0(\alpha a) \mathbf{l} \cdot V_0, \quad (\text{A } 14) \\ K_1(\alpha a) \boldsymbol{\Psi}_{\pm 1}(\kappa) &= \mp \frac{1}{2} \alpha^2 a K_1(\alpha a) (\mathbf{m} \pm \mathbf{in}) \cdot V_0 \delta'(\kappa) \\ &\quad + (\mathbf{m} \pm \mathbf{in}) (\mathbf{m} \mp \mathbf{in}) \cdot \left\{ \frac{1}{4} \alpha^2 a^2 K_3(\alpha a) V_{\pm 1} + W_{\pm 1} \right\} \delta(\kappa) \\ &\quad + \{ \mathbf{l} + \frac{1}{2} (\mathbf{m} \mp \mathbf{in}) (\mathbf{m} \pm \mathbf{in}) \} \cdot W_{\pm 1} \delta(\kappa), \end{aligned}$$

and for $j > 1$

$$\begin{aligned} K_j(\alpha a) \boldsymbol{\Psi}_{\pm j}(\kappa) &= \{ \mathbf{l} + (\mathbf{m} \pm \mathbf{in}) (\mathbf{m} \mp \mathbf{in}) \} \cdot W_{\pm j} \delta(\kappa) \\ &\quad - \frac{\alpha^2 a^2}{2j-2} K_j(\alpha a) (\mathbf{m} \mp \mathbf{in}) (\mathbf{m} \mp \mathbf{in}) \cdot V_{\pm(j-2)} \delta(\kappa) \\ &\quad + \frac{\alpha^2 a^2}{2j+2} K_{j+2}(\alpha a) (\mathbf{m} \pm \mathbf{in}) (\mathbf{m} \mp \mathbf{in}) \cdot V_{\pm j} \delta(\kappa). \end{aligned}$$

With the use of (A 10), it can be seen that these last equations contain the results of Howells (1974, §4), for the drag on an infinite cylinder in a flow independent of x , subject to Brinkman's equation. The derivative of the δ -function that occurs in $\boldsymbol{\Psi}_{\pm 1}$

arises from the linear dependence of pressure on x when there is a uniform flow at infinity.

Appendix B. Interaction between oblique cylinders

The drag force per unit area acting on the surface of rod 1 has Fourier transform $\mu a^{-1} \Psi_j(\kappa)$ (see (A 6)). $\Psi_j(\kappa)$ can be regarded as the sum of a series of reflections:

$$\begin{aligned} \Psi_j(\kappa) &= \Psi_j^{(0)}(\kappa) + \Psi_j^{(1)}(\kappa) + \sum_{r=2}^{\infty} \Psi_j^{(r)}(\kappa) \\ &= \Psi_j^{(0)}(\kappa) + \Psi_j^{(1)}(\kappa) + \Psi_j''(\kappa), \end{aligned} \quad (\text{B } 1)$$

where $\Psi_j^{(0)}(\kappa)$ represents the forces arising from the main flow in the absence of a second test rod, $\Psi_j^{(1)}(\kappa)$ the forces at rod 1 arising from the first reflection of the main flow in rod 2, $\Psi_j^{(2)}(\kappa)$ the forces arising from the second reflection – in rod 1 then in rod 2 – and so on. $\Psi_j'(\kappa)$ is the sum of the first- and higher-order reflections; $\Psi_j''(\kappa)$ is the sum of the second- and higher-order reflections, and it is this latter that is required for the second-stage calculation of mean drag.

As before, the two cylinders inclined at angle θ define orthonormal triads $\mathbf{l}, \mathbf{m}, \mathbf{n}$ and $\mathbf{l}', \mathbf{m}', \mathbf{n}'$. The axes have common normal OO' of length h in direction $\mathbf{n} = -\mathbf{n}'$. Let O_0 , the mid-point of the common normal as in figure 6, be the origin of the axes of symmetry specified by the triad $\mathbf{l}_0, \mathbf{m}_0, \mathbf{n}$. The first two of these are the respective bisectors of the angles formed by \mathbf{l}, \mathbf{l}' and by $\mathbf{m}, -\mathbf{m}'$. The velocity at infinity is to be taken, in turn, along these three axes:

$$(\text{A}) \quad \mathbf{U} = U_1 \mathbf{l}_0, \quad (\text{B}) \quad \mathbf{U} = U_2 \mathbf{m}_0, \quad (\text{C}) \quad \mathbf{U} = U_3 \mathbf{n}$$

so that three basic solutions result, from which the general solution can be formed by superposition.

Each of these basic solutions is to be expressed as a linear combination of $\mathbf{l}, \mathbf{m}, \mathbf{n}$. Thus the general solution can be written in terms of the dimensionless scalar functions $\{\Delta_{rs}(\kappa, j), r, s = 1, 2, 3\}$ of the real wavenumber κ and the integer wavenumber j :

$$\begin{aligned} \Psi_j(\kappa) &= \{\Delta_{11}(\kappa, j) \mathbf{l} + \Delta_{21}(\kappa, j) \mathbf{m} - i\Delta_{31}(\kappa, j) \mathbf{n}\} \mathbf{l}_0 \cdot \mathbf{U}a \\ &\quad + \{\Delta_{12}(\kappa, j) \mathbf{l} + \Delta_{22}(\kappa, j) \mathbf{m} - i\Delta_{32}(\kappa, j) \mathbf{n}\} \mathbf{m}_0 \cdot \mathbf{U}a \\ &\quad + \{i\Delta_{13}(\kappa, j) \mathbf{l} + i\Delta_{23}(\kappa, j) \mathbf{m} + \Delta_{33}(\kappa, j) \mathbf{n}\} \mathbf{n} \cdot \mathbf{U}a. \end{aligned} \quad (\text{B } 2)$$

Symmetry properties are expressed by the statements that the $\Delta_{rs}(\kappa, j)$ are all real, and that the above expression is replaced by its complex conjugate when the signs of κ and j are both changed. (Note the first two members of the third row and the third column are imaginary.)

The set of integral equations for $\Psi_j(\kappa)$ involves three sets of operators:

(i) The operator \mathcal{S} first reverses the \mathbf{m}_0, \mathbf{n} components of the main flow (uniform at infinity), and then rotates the entire system through 180° about \mathbf{l}_0 . This leaves the flow field unchanged, but takes any point on one rod into the point with the same coordinates on the other, interchanges the triads $\mathbf{l}, \mathbf{m}, \mathbf{n}$ and $\mathbf{l}', \mathbf{m}', \mathbf{n}'$, and takes the stress distribution over one rod into that over the other. Thus if $\Psi = \{\Psi_j(\kappa)\}$ represents the Fourier transform of the stress distribution on the rod at $\mathbf{l}, \mathbf{m}, \mathbf{n}$, then $\mathcal{S}\Psi$ represents the same for the rod at $\mathbf{l}', \mathbf{m}', \mathbf{n}'$.

(ii) The operators \mathcal{V}, \mathcal{W} are defined by (A 4)–(A 5); they give the ‘potentials’ $\Pi = \{\Pi_j(\kappa)\}$, $\Omega = \{\Omega_j(\kappa)\}$ for the flow at rod 1 as a result of stress $\Phi = \{\Phi_n(\kappa)\} = -\mathcal{S}\Psi$ acting on the fluid at rod 2:

$$\Pi = \mathcal{V}\Phi = -\mathcal{V}\mathcal{S}\Psi, \quad \Omega = \mathcal{W}\Phi = -\mathcal{W}\mathcal{S}\Psi.$$

(iii) The operator \mathcal{T} is defined by (A 7)–(A 9); it gives the stress distribution over rod 1 as a result of the above flow, denoted $\Psi_{refl.}$ to indicate that it is the reflection of the stress distribution Ψ :

$$\Psi_{refl.} = \mathcal{T}\{\Pi, \Omega\} = -\mathcal{T}\{\mathcal{V}\mathcal{S}\Psi, \mathcal{W}\mathcal{S}\Psi\}.$$

Then the set of integral equations for $\Psi'' = \{\Psi''_j(\kappa)\}$, the contribution from second and higher reflections to the stress on the rods in a uniform flow, is obtained by setting $\Psi_{refl.} = \Psi''$, $\Psi = \Psi' = \Psi'' + \Psi^{(1)}$:

$$\Psi'' = -\mathcal{T}\{\mathcal{V}\mathcal{S}\Psi'', \mathcal{W}\mathcal{S}\Psi''\} - \mathcal{T}\{\mathcal{V}\mathcal{S}\Psi^{(1)}, \mathcal{W}\mathcal{S}\Psi^{(1)}\}, \quad (\text{B } 3)$$

where

$$\Psi^{(1)} = -\mathcal{T}\{\mathcal{V}\mathcal{S}\Psi^{(0)}, \mathcal{W}\mathcal{S}\Psi^{(0)}\},$$

and $\Psi^{(0)}$ represents the stress on rod 1 due to the main flow.

In a uniform main flow U , see (A 13)–(A 14)

$$\left. \begin{aligned} \Psi_0^{(0)}(\kappa) &= 2\{C_L \mathbf{I} + C_T(\mathbf{J} - \mathbf{I})\} \cdot U\delta(\kappa), \\ \Psi_{\pm 1}^{(0)}(\kappa) &= -\frac{1}{2}\alpha^2 a(\pm \mathbf{m} + \mathbf{in}) \mathbf{l} \cdot U\delta'(\kappa), \\ \Psi_{\pm 2}^{(0)}(\kappa) &= -\frac{1}{2}\alpha^2 a^2(\pm \mathbf{m} - \mathbf{in})(\pm \mathbf{m} - \mathbf{in}) \cdot U\delta(\kappa). \end{aligned} \right\} \quad (\text{B } 4)$$

For numerical computation, the general stress distribution Ψ'' corresponding to second and higher reflections is expressed as in (B 2) in terms of the scalar components $\Delta''_{rs}(\kappa, j)$. The following set of equations, for $s = 1, 2, 3$, relate the $\Delta''_{rs}(\kappa, j)$ to $\Delta'_{rs}(\kappa, j) = \Delta''_{rs}(\kappa, j) + \Delta^{(1)}_{rs}(\kappa, j)$. They are to be solved for the $\Delta''_{rs}(\kappa, j)$, given the first reflection $\Delta^{(1)}_{rs}(\kappa, j)$:

$$\left. \begin{aligned} H_{1s}(\kappa, j) &= |\kappa|^{-1} \int_{-\infty}^{\infty} \sum_{n=-\infty}^{\infty} F_{jn}(\kappa, \kappa'; 0) \{ \kappa' \Delta'_{1s}(\kappa', n) + \kappa'' \Delta'_{2s}(\kappa', n) + q \Delta'_{3s}(\kappa', n) \} d\kappa', \\ H_{2s}(\kappa, j) &= \kappa_\alpha^{-2} \int_{-\infty}^{\infty} \sum_{n=-\infty}^{\infty} F_{jn}(\kappa, \kappa'; \alpha) \{ (\kappa\kappa' + \alpha^2 \cos \theta) \Delta'_{1s}(\kappa', n) \\ &\quad + (\kappa\kappa'' + \alpha^2 \sin \theta) \Delta'_{2s}(\kappa', n) + \kappa q_\alpha \Delta'_{3s}(\kappa', n) \} d\kappa', \\ H_{3s}(\kappa, j) &= \kappa_\alpha^{-1} \int_{-\infty}^{\infty} \sum_{n=-\infty}^{\infty} F_{jn}(\kappa, \kappa'; \alpha) \{ q_\alpha \sin \theta \Delta'_{1s}(\kappa', n) \\ &\quad - q_\alpha \cos \theta \Delta'_{2s}(\kappa', n) + \kappa''' \Delta'_{3s}(\kappa', n) \} d\kappa', \end{aligned} \right\} \quad (\text{B } 5)$$

$$\left. \begin{aligned} \varepsilon_s |\sin \theta| K_j(\kappa_\alpha a) G_{j-1}(\kappa) \{ \Delta''_{2s}(\kappa, j) + \Delta''_{3s}(\kappa, j) \} &= H_{1s}(\kappa, j-1) \\ &\quad - \text{sgn}(\kappa) M_{j-1}(\kappa) H_{2s}(\kappa, j-1) - \{ M_{j-2}(\kappa) - |\kappa/\kappa_\alpha| M_{j-1}(\kappa) \} H_{3s}(\kappa, j-1), \\ \varepsilon_s |\sin \theta| K_j(\kappa_\alpha a) G_j(\kappa) \Delta''_{1s}(\kappa, j) &= (\kappa/\kappa_\alpha) H_{1s}(\kappa, j) \\ &\quad - \frac{1}{2} \{ M_{j-1}(\kappa) + M_{j+1}(\kappa) \} H_{2s}(\kappa, j) + \frac{1}{2} (\kappa/\kappa_\alpha) \{ M_{j-1}(\kappa) - M_{j+1}(\kappa) \} H_{3s}(\kappa, j), \\ \varepsilon_s |\sin \theta| K_j(\kappa_\alpha a) G_{j+1}(\kappa) \{ \Delta''_{2s}(\kappa, j) - \Delta''_{3s}(\kappa, j) \} &= -H_{1s}(\kappa, j+1) \\ &\quad + \text{sgn}(\kappa) M_{j+1}(\kappa) H_{2s}(\kappa, j+1) - \{ M_{j+2}(\kappa) - |\kappa/\kappa_\alpha| M_{j+1}(\kappa) \} H_{3s}(\kappa, j+1), \end{aligned} \right\} \quad (\text{B } 6)$$

where

$$F_{jn}(\kappa, \kappa'; \alpha) = \left(\frac{q_\alpha - \kappa''}{\kappa_\alpha} \right)^j \left(\frac{q_\alpha - \kappa''}{\kappa'_\alpha} \right)^n I_n(\kappa'_\alpha a) q_\alpha^{-1} e^{-q_\alpha h},$$

$$F_{jn}(\kappa, \kappa'; 0) = \left(\frac{q - \kappa''}{|\kappa|} \right)^j \left(\frac{q - \kappa''}{|\kappa'|} \right)^n I_n(|\kappa'| a) q^{-1} e^{-qh},$$

$$G_j(\kappa) = M_{j-1}(\kappa) - 2|\kappa/\kappa_\alpha| M_j(\kappa) + M_{j+1}(\kappa), \quad M_j(\kappa) = K_j(|\kappa| a) / K_j(\kappa_\alpha a),$$

$$\varepsilon_s = 1 \quad \text{for } s = 1, \quad \varepsilon_s = -1 \quad \text{for } s = 2, 3,$$

and see (A 5).

αa	1/8	1/2	2
$\int_0^{\pi/2} R_1 d\theta$	2.035	0.335	0.031
$\int_0^{\pi/2} 2S_1 d\theta$	1.184	0.745	0.334
Q_1	3.219	1.080	0.365
$\int_0^{\pi/2} R_2 d\theta$	5.818	2.163	1.621
$\int_0^{\pi/2} 2S_2 d\theta$	1.444	1.460	3.230
Q_2	7.262	3.623	4.851
$(Q_1 + 2Q_2)/3$	5.914	2.775	3.356

TABLE 3. Results of calculation for oblique rod interaction

These are solved by iteration. When h , the separation of the rods, is large enough only a few iterations are needed, and only one or two orders of Fourier components around the rods. But as h approaches its lower bound $2a$, a greater number of the azimuthal Fourier components are needed, and more iterations. Then convergence is accelerated by use of the technique of under-relaxation, as shown by the scheme

$$y_{n+1} = rF(y_n) + (1-r)y_n,$$

where F is the operator for iteration, y_n the n th iteration, and r is the relaxation coefficient. Ordinary iteration is given by $r = 1$, under-relation by $r < 1$.

Calculations were performed at the values $\alpha a = \frac{1}{8}, \frac{1}{2}, 2$, for $\theta = \frac{1}{6}\pi, \frac{1}{3}\pi, \frac{1}{2}\pi$, and for a sufficient set of values of $\eta = h/a \geq 2$ to permit an approximate evaluation of the integrals of $\Psi_0''(0)$ that are needed for the second-stage drag calculation set out in §5.

The integral over ϕ , the azimuthal angle about \mathbf{l} of the common normal to the two rods, can be written down as follows:

$$\left. \begin{aligned} \sin^2 \theta \int_0^{2\pi} \Psi_0''(0) d\phi &= \pi a U \cdot \{S_1(\eta, \theta, \alpha a) \mathbf{ll} + S_2(\eta, \theta, \alpha a) (\mathbf{l} - \mathbf{ll})\}, \\ \text{where} \quad S_1(\eta, \theta, \alpha a) &= 2\{D_{11}(\eta, \theta) \cos \frac{1}{2}\theta - D_{12}(\eta, \theta) \sin \frac{1}{2}\theta\} \sin^2 \theta, \\ S_2(\eta, \theta, \alpha a) &= \{D_{21}(\eta, \theta) \sin \frac{1}{2}\theta + D_{22}(\eta, \theta) \cos \frac{1}{2}\theta + D_{33}(\eta, \theta)\} \sin^2 \theta, \end{aligned} \right\} \quad (\text{B } 7)$$

and $D_{rs}(\eta, \theta) = D_{rs}''(j=0, \kappa=0)$ as a function of $\eta = h/a$, θ , in terms of the solutions to (B 5).

Further write

$$R_k(\theta, \alpha a) = \int_2^\infty S_k(\eta, \theta, \alpha a) d\eta,$$

and then

$$Q_k(\alpha a) = \int_0^{\pi/2} \{R_k(\theta, \alpha a) + 2S_k(2, \theta, \alpha a)\} d\theta, \quad k = 1, 2,$$

are the quantities that appear in the drag evaluation in §5. See table 3.

Limiting cases:

(i) αa large. The limiting case is that of simple Darcy law flow past two inclined cylinders. The pressure force from second and higher reflections will be of order $\mu\alpha^2 Ua^6 h^{-3}$ (shearing force will be of order $\mu\alpha Ua^3 h^{-3}$). Orders of magnitude of both R_2 and S_2 are $\alpha^2 a^2$.

(ii) αa small. Orders of magnitude of R_2, S_2 are $(\alpha a)^{-2}\{K_0(\alpha a)\}^{-3}, (\alpha a)^{-1}\{K_0(\alpha a)\}^{-3}$.

(iii) θ small. In terms of the corresponding drag coefficients d_{11}, d_{22}, d_{33} on pairs of parallel rods, a distance r apart,

$$\sin \theta D_{jk}(h/a, \theta) \rightarrow \delta_{jk} \int_h^\infty 2 d_{kk}(r/a) \frac{r dr}{(r^2 - h^2)^{1/2}}.$$

REFERENCES

- ACRIVOS, A., HINCH, E. J. & JEFFREY, D. J. 1980 Heat transfer to a slowly moving fluid from a dilute fixed bed of heated spheres. *J. Fluid Mech.* **101**, 403–421.
- ACRIVOS, A. & SHAQFEH, E. S. G. 1988 The effective thermal conductivity and elongational viscosity of a non-dilute suspension of aligned slender rods. *Phys. Fluids* **31**, 1841–1844.
- BACHELOR, G. K. 1971 The stress generated in a non-dilute suspension of elongated particles by pure straining motion. *J. Fluid Mech.* **46**, 813–829.
- BACHELOR, G. K. 1972 Sedimentation in a dilute dispersion of spheres. *J. Fluid Mech.* **52**, 245–268.
- BIXON, M. & ZWANZIG, R. 1981 Diffusion in a medium with static traps. *J. Chem. Phys.* **75**, 2354–2356.
- BRINKMAN, H. C. 1947 A calculation of the viscous force exerted by a flowing fluid on a dense swarm of particles. *Appl. Sci. Res. A* **1**, 27.
- CHILDRESS, S. 1972 Viscous flow past a random array of spheres. *J. Chem. Phys.* **56**, 2527.
- CLAGUE, D. S. & PHILLIPS, R. J. 1996 Hindered diffusion of spherical macromolecules through dilute fibrous media. *Phys. Fluids* **8**, 2720–2731.
- DAVIES, C. N. 1952 The separation of airborne dust and particles. *Proc. Inst. Mech. Engrs* **1B**, 185–198.
- EVANS, A. R., SHAQFEH, E. S. G. & FRATTINI, P. L. 1994 Observations of polymer conformation during flow through a fixed fibre bed. *J. Fluid Mech.* **281**, 319–356.
- FRATTINI, P. L., SHAQFEH, E. S. G., LEVY, J. L. & KOCH, D. L. 1991 Observations of axisymmetric tracer particle orientation during flow through a dilute fixed bed of fibers. *Phys. Fluids A* **3**, 2516–2528.
- FREDRICKSON, G. H. & SHAQFEH, E. S. G. 1989 Heat and mass transport in composites of aligned slender fibers. *Phys. Fluids A* **1**, 3–20.
- GHADDAR, C. K. 1995 On the permeability of unidirectional fibrous media: a parallel computational approach. *Phys. Fluids* **7**, 2563–2586.
- HINCH, E. J. 1977 An averaged-equation approach to particle interactions in a fluid suspension. *J. Fluid Mech.* **83**, 695–720.
- HOWELLS, I. D. 1974 Drag due to the motion of a Newtonian fluid through a sparse random array of small fixed rigid objects. *J. Fluid Mech.* **64**, 449–475.
- KANEDA, Y. 1986 The drag on a sparse random array of fixed spheres in flow at small but finite Reynolds number. *J. Fluid Mech.* **167**, 455–463.
- KIRKPATRICK, T. R. 1982 Time dependent transport in a fluid with static traps. *J. Chem. Phys.* **76**, 4255–4259.
- MUTHUKUMAR, M. 1982 Concentration dependence of diffusion controlled processes among static traps. *J. Chem. Phys.* **76**, 2667–2671.
- O'BRIEN, R. W. 1979 A method for the calculation of the effective transport properties of suspensions of interacting particles. *J. Fluid Mech.* **91**, 17–39.
- SCHIEK, R. L. & SHAQFEH, E. S. G. 1995 A non-local theory for stress in bound, Brownian suspensions of slender, rigid fibres. *J. Fluid Mech.* **296**, 271–324.
- SHAQFEH, E. S. G. 1988 A non-local theory for the heat transport in composites containing highly conducting fibrous inclusions. *Phys. Fluids* **31**, 2405–2425.

- SHAQFEH, E. S. G. & FREDRICKSON, G. H. 1990 The hydrodynamic stress in a suspension of rods. *Phys. Fluids A* **2**, 7–24.
- SHAQFEH, E. S. G. & KOCH, D. L. 1988 The effects of hydrodynamic interactions on the orientation of axisymmetric particles flowing through a fixed bed of spheres or fibers. *Phys. Fluids* **31**, 728–743.
- SHAQFEH, E. S. G. & KOCH, D. L. 1992 Polymer stretch in dilute fixed beds of spheres or fibers. *J. Fluid Mech.* **244**, 17–54.
- SPIELMAN, L. & GOREN, S. L. 1968 Model for predicting pressure drop and filtration efficiency in fibrous media. *Environ. Sci. Technol.* **2**, 279–287.
- WILLIS, J. R. & ACTON, J. R. 1976 The overall elastic moduli of a dilute suspension of spheres. *Q. J. Mech. Appl. Maths* **29**, 163.